Models for the architecture of the human inner kinetochore CCAN complex on centromeric α-satellite CENP-A nucleosome arrays

Cong Yu[1], Kyle W. Muir[1,3], Jing Yang[1], Ziguo Zhang[1], Stephen H. McLaughlin[1] and David Barford[1,2]

[1]MRC Laboratory of Molecular Biology, Francis Crick Avenue, Cambridge, CB2 0QH, UK

[2]Corresponding author: dbarford@mrc-lmb.cam.ac.uk

[3]Present address: Institute of Cell Biology, University of Edinburgh, Edinburgh, UK.

Abstract

Human kinetochores assemble onto centromeric DNA defined by tandem copies of thousands of the 171 bp α-satellite repeat sequence. The centromere-specific CENP-A nucleosome (CENP-A^{Nuc}) recruits the inner kinetochore constitutive centromere associated network (CCAN) complex. A previous cryo-EM structure of CCAN bound to a CENP-A^{Nuc} reconstituted with a 171 bp α-satellite repeat sequence showed how extranucleosomal linker DNA threads through an internal tunnel in the CCAN complex. To understand the higher-order architecture of the inner kinetochore assembled onto α-satellite repeat arrays we have determined cryo-EM structures of CCAN with longer DNA sequences. These include free DNA and single and dimeric α-satellite repeats with CENP-A nucleosomes. We show from the structures of CCAN bound to both free DNA and monomeric CENP-A^{Nuc} that CCAN engages 65-70 bp of DNA comprising 30-35 bp of an upstream α-satellite repeat. This upstream DNA interacts with the histone fold domain subunits of the CENP-TWSX module in a manner resembling how DNA is wrapped in nucleosomes. A complex of CCAN assembled onto a dimeric α-satellite repeat with two CENP-A nucleosomes showed that CCAN can only be accommodated on the linker DNA by unwrapping DNA from the CENP-TWSX module together with 25 bp of DNA from the upstream nucleosome. We discuss the implications of these results for models of CCAN assembly on arrays of α-satellite chromatin containing CENP-A^{Nuc}.

Introduction

The faithful inheritance of genetic information is crucial for life. Central to this process in eukaryotes are the roles fulfilled by kinetochores – large protein complexes that assemble

at centromeric chromatin. Kinetochores function to attach sister chromatids to the mitotic spindle, and couple the work of microtubule depolymerization to chromatid segregation [1-3]. Kinetochores also act as signalling hubs for the error correction and spindle assembly checkpoints that together coordinate the correct attachment of sister chromatids to the mitotic spindle with the initiation of sister chromatid segregation [4,5].

Human regional centromeres are megabase-sized structures, comprising thousands of contiguous 171 bp α-satellite repeat sequences. Identical α-satellite repeats are organized into higher order repeat (HOR) arrays of typically four, seven and eleven repeats [6]. Only a small fraction of α-satellite repeats is associated with the approximately four-hundred CENP-A nucleosomes per centromere [7]. CENP-A nucleosomes are restricted to the hypo-methylated centromere dip region (CDR), the most recently evolved segment of centromeres [6,8,9], and are interspersed with canonical H3 nucleosomes [10]. Assuming at most 147 bp of DNA wraps a histone octamer [11], at least 24 bp of α-satellite repeat sequence forms extranucleosomal linker DNA. Both *in vivo* ChIP-seq mapping and in *vitro* reconstitution of CENP-A nucleosomes on α-satellite sequences indicate that the CENP-A nucleosome is installed precisely towards the 3' end of the repeat, with the centre of the α-satellite repeat palindrome coinciding with the nucleosome dyad axis [12,13]. Human centromeres, except for the Y chromosome centromere, contain the 17 bp B-box element. The majority of B-boxes are arranged on alternating α-satellite repeats [14] positioned such that the B-box on linker DNA partially overlaps a nucleosome entry site [15]. CENP-B engagement by the B-box facilitates unwrapping of the DNA gyre from the CENP-A histone octamer [16], whereas the engagement of the dimeric CENP-B to two separate B-boxes induces looping of centromeric DNA [17].

The centromere-kinetochore assembly of vertebrates comprises large macromolecular complexes at the constriction point of chromosomes visible by electron microscopy in prometaphase cells as plate-like structures ~200 nm in diameter, and attached to 20-30 microtubule filaments [18]. Kinetochores are composed of two main components: the inner kinetochore centromere-binding CCAN complex, and the microtubule-binding KMN complex of the outer kinetochore [19]. The 16-subunit CCAN complex is organized into five modules: CENP-C and CENP-OPQUR, and the DNA-binding modules, CENP-LN, CENP-HIKM and CENP-TWSX. The latter module comprises four histone fold domain proteins [20]. Cryo-EM structures of human and budding yeast CCAN have elucidated mechanisms of centromere and CENP-A nucleosome recognition [12,21-25]. CCAN encloses extranucleosomal linker DNA within a topologically-enclosed chamber [12,22], a mechanism recently shown to be conserved in the CENP-A-independent holocentric kinetochores of *Lepidoptera* [26]. In vertebrates,

interactions with the CENP-A nucleosome, that confer CCAN specificity for CENP-A rather than H3 nucleosomes, are mediated primarily by the CENP-C subunit through its short linear interaction motifs that bridge the CENP-A histone of CENP-A^{Nuc} with the CCAN modules CENP-LN and CENP-HIKM [12,21,23,27-30]. Human CENP-C incorporates two CENP-A-binding motifs, generating four potential CENP-A-binding sites in the CENP-C dimer [31].

In our previous cryo-EM structures of CCAN:CENP-A^{Nuc} and CCAN:DNA complexes, a DNA duplex was observed threading through a 50 Å-long central tunnel running the length of the CCAN molecule [12]. This DNA-binding tunnel is formed by the CENP-LN channel, and CENP-I and CENP-TW subunits. As the DNA exits the tunnel it curves around the CENP-TWSX module, interacting with the histone fold domains of CENP-TW. The DNA molecules used in the earlier study (the 171 bp α-satellite DNA used to reconstitute the CENP-A^{Nuc} for the CCAN:CENP-A^{Nuc} complex, and the 54 bp DNA used in the CCAN:DNA complex) were of insufficient length to extend beyond CENP-TW, and so in these complexes DNA did not contact CENP-SX of the histone-fold CENP-TWSX module. Previous cell biology and biochemical studies however, had identified CENP-SX as DNA-binding proteins at the centromere [32]. We were therefore missing important details regarding how CCAN interacts with DNA at the centromere, and this information is required for understanding the higher-order architecture of kinetochores arranged on α-satellite repeat arrays. Furthermore, the repeating CCAN:CENP-A nucleosome unit at centromeres is not defined. Thus, the aims of this study are two-fold. First, we aim to obtain a more complete understanding of how CCAN interacts with DNA, and second we seek to provide models for how multiple copies of CCAN and CENP-A nucleosomes assemble onto contiguous α-satellite repeat sequences at human centromeres.

Results

CCAN binds 70 bp of DNA in a loop configuration that wraps the CENP-TWSX module

To understand how centromeric DNA interacts with CCAN, including all of the histone fold domains (HFDs) of the CENP-TWSX module, we reconstituted CCAN with a longer DNA duplex (human α-satellite DNA: 171 bp) and used mild cross-linking to stabilize the complex. The cryo-EM structure, resolved to 3.3 Å resolution, showed clearly defined cryo-EM density for ~70 bp of DNA that wraps around CCAN in a loop-like structure (**Fig. 1 and Extended Data Fig. 1 and Extended Data Table 1**). As observed in our previous CCAN:CENP-A^{Nuc} and CCAN:DNA complexes [12], DNA threads through the enclosed CCAN chamber, contacting CENP-TW as it exits the tunnel (**Fig. 1**). However, in the new structure, we observed an additional 20 bp of DNA exiting the DNA-binding tunnel, so that in total 40 bp of DNA

interacts with the entire CENP-TWSX module. Additionally, a short segment of DNA (~5 bp) extends beyond the CENP-TWSX module and approaches CENP-QU.

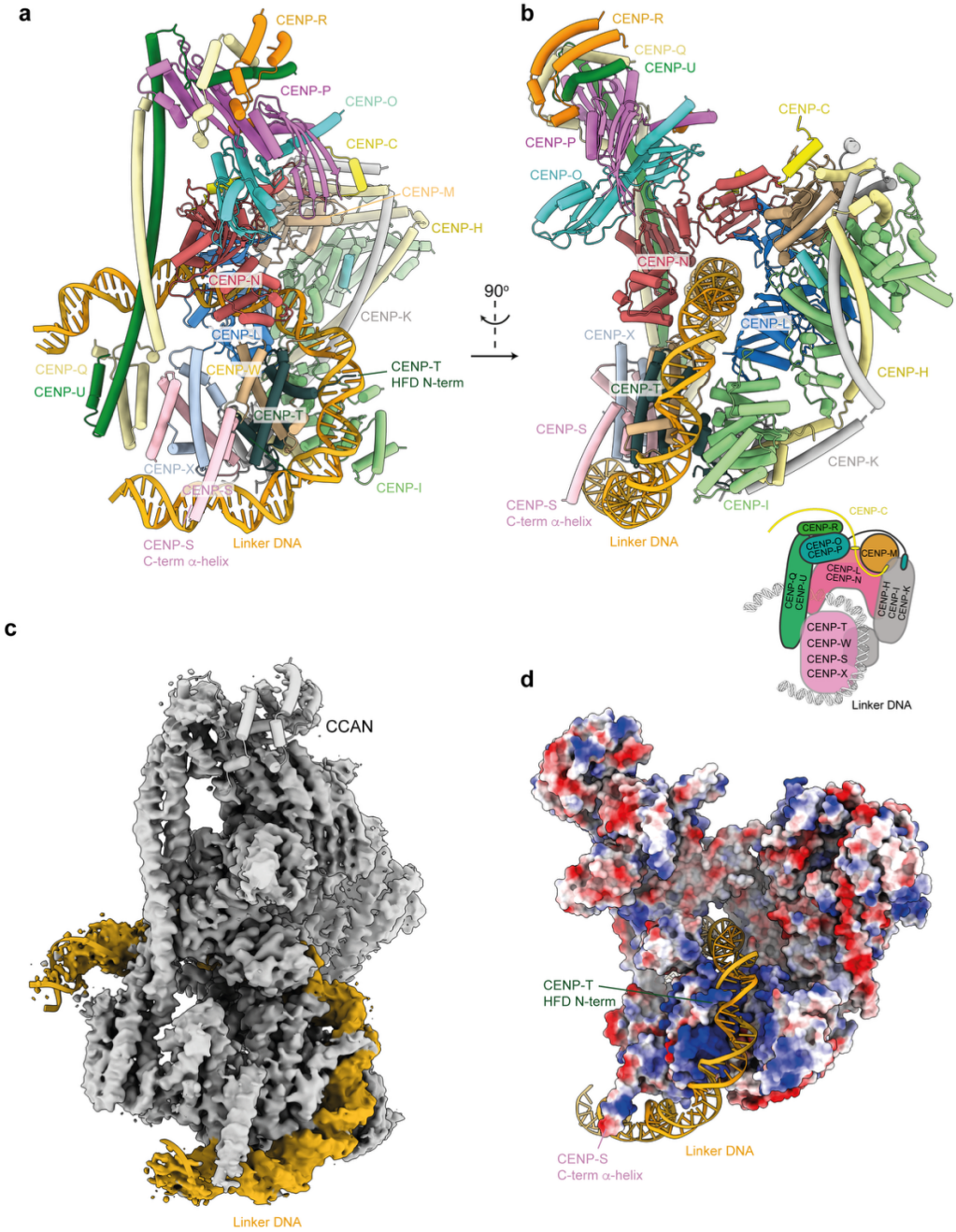

Fig. 1. CCAN binds 70 bp of DNA in a loop configuration. **a** and **b**, Orthogonal views of the CCAN:DNA complex. 41 bp of DNA interacts with the CENP-TWSX module. Insert: Schematic of the CCAN:DNA complex. **c**, Cryo-EM map of the CCAN:DNA complex with DNA coloured in gold and CCAN subunits in grey. **d**, Electrostatic surface of CCAN as viewed in panel B, with DNA shown as a ribbons representation.

The HFDs of the CENP-TWSX module assemble into a heterotetramer that structurally resembles the H3:H4 tetramer of canonical nucleosomes (**Fig. 2a, b**) [11,32]. In the CCAN:DNA

complex, DNA wraps around CENP-TWSX comparably to how H3:H4 tetramers wrap DNA in the context of an octameric nucleosome [11]. In both structures DNA has a similar curvature and adopts a left-handed helical geometry. The CENP-TWSX module creates a positively-charged ridge that binds the DNA phosphate backbone (**Fig. 1d**). Strikingly, DNA wraps the H3:H4 and CENP-TWSX tetramers with identical registers such that the DNA major groove projects towards both the dyad axis of the H3:H4 tetramer, and the related pseudo-dyad axis of CENP-TWSX (**Fig. 2a, b**). Consequently, in both structures, at superhelical locations (SHLs) ±0.5, ±1.5, ±2.5, the DNA minor groove projects towards and contacts equivalent residues in the histone fold domains of the H3:H4 tetramer and CENP-TWSX module. Our structure shows that DNA interacts with conserved basic residues of all four HFD domains of CENP-TWSX (**Fig. 2c, d**), consistent with prior mutagenesis data demonstrating the role of basic CENP-TWSX amino acids in DNA binding *in vitro* and centromere localization *in vivo* [20,32].

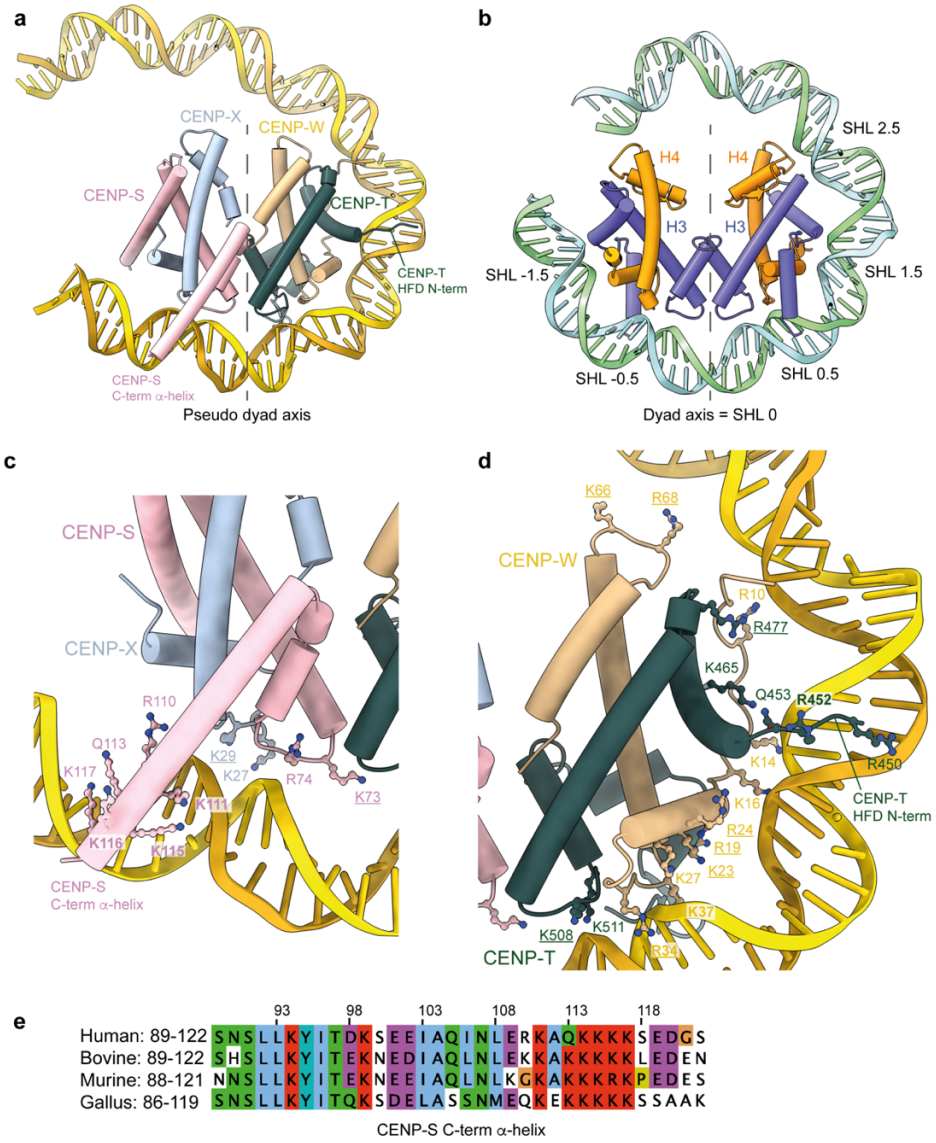

Fig. 2. The CENP-TWSX module binds DNA analogous to the H3:H4 histone tetramer of canonical nucleosomes. a, CENP-TWSX and CCAN-associated 70 bp DNA, 40 bp interacts with the CENP-TWSX

module. **b**, H3:H4 tetramer of a nucleosome with almost with 67 bp of DNA. Super helical locations (SHLs) are indicated. The pseudo dyad axes of CENP-TWSX and the H3:H4 tetramer are shown in A and B (PDB: [11]). **c**, Details of basic residues from the HFDs of CENP-S and CENP-X and CENP-S C-terminal α-helix interacting with the DNA phosphate backbone. **d**, Details of basic residues from the HFDs of CENP-T and CENP-W, and CENP-T N-terminal extension interacting with the DNA phosphate backbone. In (C) and (D) residues previously shown to contribute to CENP-TWSX – DNA binding are underlined [32]. **e**, Multiple sequence alignment of the CENP-S C-terminal α-helix. Alignment created using Jalview [33].

Additional protein-DNA contacts stabilize CENP-TWSX – DNA interactions. These involve an extended basic segment immediately N-terminal of the CENP-T HFD that inserts into the DNA minor groove, and a C-terminus α-helix of CENP-S that engages the DNA major groove (**Fig. 2a, c and d**). This CENP-S α-helix becomes ordered on binding DNA, such that a conserved stretch of basic residues stabilize its interactions with the DNA backbone (**Fig. 2c, e**), as similarly observed in the crystal structure of a CENP-SX:DNA complex [34]. Our structural data are consistent with previous studies showing that deletion of the C-terminus of CENP-S, including this basic region, abolished CENP-S binding to DNA *in vitro* [32]. Similar observations regarding the interaction of linker DNA with the CENP-TWSX module were obtained by Musacchio and colleagues from a cryo-EM structure of a CCAN:DNA complex (M. Pesenti, I. Vetter and A. Musacchio, unpublished data).

<u>DNA of CENP-A^{Nuc} reconstituted with longer α-satellite repeat DNA wraps CENP-TWSX</u>

We next assessed whether CENP-TWSX wraps linker DNA in the context of a CENP-A nucleosome. We assembled CCAN onto a CENP-A^{Nuc} reconstituted with 211 bp DNA that comprised the 171 bp α-satellite repeat and 40 bp from the 5' upstream α-satellite repeat, and determined its structure using cryo-EM to an overall resolution of 4.5 Å (**Extended Data Fig. 2**). Both individual CCAN:DNA and CENP-A^{Nuc} modules were resolved in cryo-EM density, showing relative flexibility (**Extended Data Fig. 2d**). A total of 200 bp DNA was visible in the cryo-EM map. Similar to our previous CCAN:CENP-A^{Nuc} structure with 171 bp DNA [12], CENP-A^{Nuc} is positioned at the 3' end of the α-satellite repeat (**Fig. 3a, c**). The 5' terminus of the CENP-A^{Nuc} DNA gyre is unwrapped by 10 bp. This unwrapped DNA then leads into extranucleosomal linker DNA that threads through the CCAN DNA-binding tunnel. On exiting the tunnel, DNA wraps around the entire CENP-TWSX module, as seen in the CCAN:DNA complex described above. This DNA comprises linker DNA of the 3' downstream α-satellite repeat together with 30 bp of the 5' upstream α-satellite repeat. Thus, a total of ~65 bp of free DNA 5' of CENP-A^{Nuc} interacts with CCAN (**Fig. 3c**). An unexpected finding was that compared with our previous CCAN:CENP-A^{Nuc} cryo-EM structure [12], CENP-A^{Nuc} adopts a different orientation relative to CCAN. In our new structure, CENP-A^{Nuc} is rotated by 216° and shifted by six bp away from CCAN. A shift of register while maintaining the same DNA

181 phosphate backbone interactions with the CCAN DNA-binding tunnel causes the DNA duplex
182 (and hence CENP-A^{Nuc}) to rotate 36° per bp, rotating 216° overall (**Fig. 3b and**
183 **Supplementary Video 1**). The reasons for the differences in CENP-A^{Nuc} position between the
184 two CCAN:CENP-A^{Nuc} complexes are not entirely clear. A possible explanation is that the
185 longer extranucleosomal DNA linker used in this study optimizes interactions with DNA-
186 binding sites on CCAN, resulting in displacement of CENP-A^{Nuc}. Cryo-EM density for CENP-C
187 is observed at the CENP-C-binding sites on CENP-A^{Nuc}, CENP-LN and CENP-HIKM, however,
188 due to the displaced CENP-A^{Nuc}, there are no direct contacts between CENP-A^{Nuc} and the
189 back-side of CCAN.

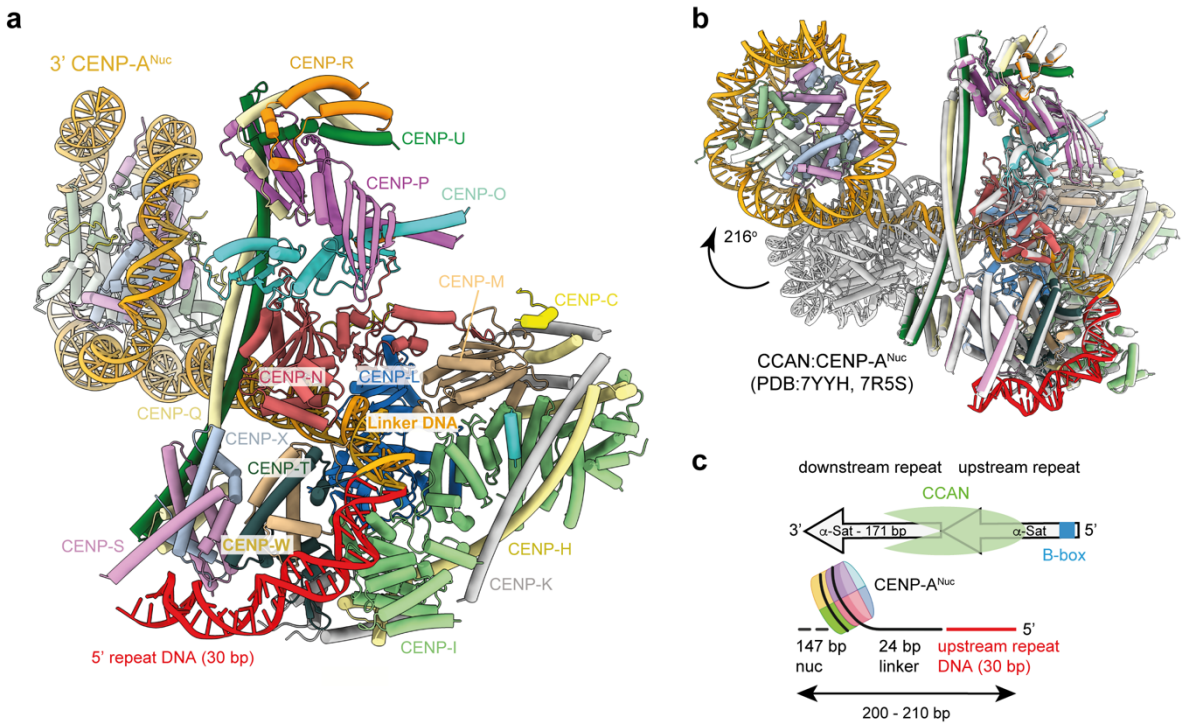

190
191
192 **Fig. 3. Cryo-EM structure of CCAN:CENP-A^{Nuc} showing CENP-TWSX binding DNA. a**, Ribbons
193 representation of the CCAN:CENP-A^{Nuc} complex. DNA coloured in red indicates DNA of the 5'
194 upstream α-satellite repeat. **b**, Superimposition of our new CCAN:CENP-A^{Nuc} complex (with 211 bp
195 DNA) (coloured as in panel A) onto the previous model of CCAN:CENP-A^{Nuc} with a single 171 bp α-
196 satellite repeat DNA (coloured grey) [12]. This shows the difference in position and orientation of the 3'
197 CENP-A^{Nuc}. The two nucleosomes differ in orientation by 216° due to a 6 bp translation of the repeat
198 sequence through the tunnel (**Supplementary Video 1**). **c**, Schematic of the CCAN:CENP-A^{Nuc} on an
199 α-satellite repeat dimer. A total of 200-210 bp of DNA is embedded by the complex including 30 bp
200 from the 5' upstream α-satellite repeat. A B-box accessible for CENP-B binding in the upstream
201 repeat is shown in blue.
202
203 Although the cryo-EM density for the DNA phosphate backbone is well resolved, density for
204 individual DNA bases is less well defined such that purine and pyrimidine bases are not
205 distinguished. We therefore do not observe sequence-specific protein-DNA interactions. In
206 conclusion, these new structures of CCAN with both free DNA and a CENP-A^{Nuc} with an

extended extranucleosomal DNA linker are consistent with earlier proposals that the CENP-TWSX module of the kinetochore functions as a nucleosome-like particle at the centromere [20,32].

Implications for CCAN binding to α-satellite repeat dimers

Our new CCAN:DNA and CCAN:CENP-A^{Nuc} structures showing that CCAN itself interacts with 65 bp of duplex DNA has implications for understanding the higher-order organization of CCAN on repetitive α-satellite repeat CENP-A nucleosome arrays. The 65 bp DNA interacting with CCAN comprises 30 bp from the 5' upstream α-satellite repeat and 35 bp of the 3' downstream α-satellite repeat: 24 bp of extranucleosomal linker DNA and 10 bp of unwrapped CENP-A^{Nuc} DNA (**Fig. 3c**). The 30 bp DNA interacting with CCAN from the 5' upstream α-satellite repeat is DNA of the CENP-A nucleosome gyre when CENP-A nucleosomes are positioned at the 3' end of the α-satellite repeat [12,13]. This suggests that in the context of a CCAN:CENP-A^{Nuc} complex, the upstream α-satellite repeat might be devoid of a nucleosome (either CENP-A or canonical H3). In alternative non-exclusive scenarios, to accommodate CCAN bound between two CENP-A nucleosomes on adjacent α-satellite repeats, a CENP-A nucleosome positioned on the upstream 5' α-satellite repeat might unwrap by 30 bp, or the upstream CENP-A^{Nuc} may force DNA to unwrap from the CENP-TWSX module. A third possibility is that CCAN repositions CENP-A^{Nuc} by causing DNA to slide around the histone octamer. However, the defined position of CENP-A^{Nuc} at the 3' of α-satellite repeats *in vivo* [13] does not support this scenario.

Substantial evidence indicates that the DNA termini of CENP-A nucleosomes are loosely wrapped and flexible. First, nuclease digestion sensitivity assays showed that CENP-A nucleosomes protect only 100-120 bp DNA, compared to 140-150 bp for canonical H3 nucleosomes [13,24,35,36]. Second, FRET data indicated increased flexibility of terminal DNA segments in CENP-A^{Nuc} relative to canonical nucleosomes [16]. Third, both crystal and cryo-EM structures of CENP-A^{Nuc} revealed unwrapping of terminal DNA segments [12,16,24,37-41], in some instances as much as 24-36 bp of flexible DNA at one end [42]. Finally, CENP-B and CENP-C have been implicated in promoting DNA unwrapping from CENP-A^{Nuc} (Refs [16,43,44]).

CCAN binds a dimeric α-satellite repeat with two CENP-A nucleosomes

To investigate the feasibility of CCAN binding to linker DNA connecting two adjacent CENP-A nucleosomes, we reconstituted two CENP-A nucleosomes on an α-satellite repeat dimer. The α-satellite repeat dimer was designed to include only linker DNA connecting the two

244 CENP-A nucleosomes: upstream and downstream α-satellite repeats were 147 bp and 171
245 bp, respectively (**Extended Data Fig. 3a**). To stabilize the two nucleosome positions on this
246 324 bp DNA, we replaced 92 bp of native α-satellite repeat DNA at the centre of each CENP-
247 A^{Nuc} site with Widom601 DNA. We observed that CCAN associated with this di-CENP-A^{Nuc}
248 array, as assessed by size exclusion chromatography (SEC) (**Extended Data Fig. 3b, c**).
249 Analysis of the peak SEC fractions using interferometric scattering microscopy (iSCAT)
250 revealed two species: the major 1,054 kDa complex corresponded to a single CCAN
251 promoter bound to the di-CENP-A^{Nuc} array (CCAN:di-CENP-A^{Nuc}), although with a lower mass
252 than the expected 1,282 kDa. The underestimate of molecular mass using ISCAT may be due
253 to the DNA component which scatters less than the globular proteins used for calibration. A
254 445 kDa component corresponded to a di-CENP-A^{Nuc} array without CCAN (expected
255 molecular mass of 431 kDa) (**Extended Data Fig. 3d**). The partial dissociation of CCAN from
256 di-CENP-A^{Nuc} is likely due to the low sample concentrations required for single molecule
257 counting in iSCAT.
258
259 *CCAN and CENP-B binding to the same linker DNA segment is mutually exclusive*
260 Our α-satellite dimer incorporated a B-box within the linker DNA of the downstream α-
261 satellite repeat connecting the two CENP-A nucleosomes (**Extended Data Fig. 4a**). SEC data
262 showed that the CENP-B protein recognized the B-box specifically because CENP-B bound to
263 the di-CENP-A^{Nuc} array with an intact B-box, but not to a di-CENP-A^{Nuc} array with a mutant B-
264 box (**Extended Data Fig. 4b, c**). We next tested whether CCAN and CENP-B bind the di-CENP-
265 A^{Nuc} array simultaneously. We observed that CCAN displaced CENP-B from the array,
266 showing that CCAN and CENP-B engagement of linker DNA is mutually exclusive (**Extended**
267 **Data Fig. 4d, e**). This is consistent with our model of CCAN:CENP-A^{Nuc} (Ref. [12]), that with
268 CCAN bound to linker DNA, the B-box is enclosed by the CCAN DNA-binding tunnel and
269 therefore inaccessible to CENP-B.
270
271 <u>CCAN binds to linker DNA in the dimeric α-satellite repeat with two CENP-A nucleosomes</u>
272
273 To understand the structural basis of how CCAN interacts with linker DNA connecting
274 adjacent CENP-A nucleosomes, we prepared cryo-EM grids with the CCAN:di-CENP-A^{Nuc}
275 complex. Despite cross-linking and the use of additives to reduce sample denaturation at
276 the air-water interface, CCAN:di-CENP-A^{Nuc} particles were not visible on either cryo-electron
277 micrographs or subsequent 2D classes of the cryo-EM dataset. We instead observed a
278 heterogeneous mixture of free DNA, CENP-A^{Nuc} and protein complexes (data not shown),
279 indicative of CCAN:di-CENP-A^{Nuc} denaturation on cryo-EM grids. To stabilize the CCAN:di-
280 CENP-A^{Nuc} complex for cryo-EM analysis, we combined it with the CENP-A nucleosome

281 stabilizing-single chain antibody fragment (ScFv) [40], omitting CENP-C due to its binding site
282 overlapping that of the ScFv (**Extended Data Fig. 5)**, and collected a large cryo-EM dataset
283 on this ScFv-stabilized CCAN:di-CENP-A^{Nuc} complex (**Extended Data Figs 6 and 7 and**
284 **Extended Data Table 1**).
285
286 2D classification of the selected particles and subsequent 3D reconstruction and
287 classification revealed a highly heterogenous mixture of molecular states (**Extended Data**
288 **Figs 6b-d and 7**). The majority of 2D classes from nearly nine million picked particles
289 comprised either free mono-CENP-A nucleosome or CCAN:DNA with no obvious associated
290 CENP-A nucleosome. *Ab initio* reconstruction and 3D refinement resulted in high resolution
291 maps of CCAN:DNA and a CENP-A mono-nucleosome with bound ScFv (2.9 Å and 2.7 Å,
292 respectively; **Extended Data Fig. 7**). The CCAN reconstruction showed DNA enclosed within
293 the DNA-binding tunnel. We re-extracted CCAN particles in RELION [45] using a larger box and
294 performed further 3D classification (**Extended Data Fig. 7**). This procedure revealed 3D
295 classes with diffuse, poorly-defined EM densities at both 3' and 5' entrances to the CCAN-
296 DNA tunnel that likely represented flexible CENP-A nucleosomes. To determine whether the
297 density at the 3' entrance corresponded to a 3' CENP-A nucleosome, we generated a wide
298 mask covering this density and performed signal-subtraction of density outside the mask.
299 Subsequent 3D reconstruction and classification of the mask-generated recentred particles
300 recovered a CENP-A nucleosome, confirming that the diffuse density observed in 2D classes
301 as CENP-A^{Nuc}. Using the corresponding unmasked particle set, we then calculated a new 3D
302 reconstruction at 9.5 Å resolution that revealed both CCAN and 3' CENP-A^{Nuc}. Consistent
303 with this reconstruction, 2D classes calculated from this particle set showed density features
304 for CCAN and 3' CENP-A^{Nuc}. A similar approach was used to analyse EM density at the 5'
305 entrance to the CCAN-DNA tunnel, resulting in a 3D reconstruction with CCAN and
306 associated 5' CENP-A^{Nuc} at 15 Å resolution (**Extended Data Fig. 7**). In the 2D class galleries
307 corresponding to both the 3' CCAN:CENP-A^{Nuc} and 5' CCAN:CENP-A^{Nuc} complexes, we
308 observed diffuse densities at the opposite end of the CCAN DNA-tunnel (i.e. 5' and 3',
309 respectively), for example **Extended Data Fig. 7i**. These particles are consistent with CCAN
310 bound to the linker DNA of the di-CENP-A^{Nuc} array. However, the small number of the
311 particles precluded a 3D reconstruction. We therefore generated a composite cryo-EM map
312 of a CCAN:di-CENP-A^{Nuc} complex from the individual 3' CCAN:CENP-A^{Nuc} and 5' CCAN:CENP-
313 A^{Nuc} maps (**Extended Data Fig. 7i** and **Fig. 4b**). One of its projected views matches an
314 experimental 2D class of a CCAN:di-CENP-A^{Nuc} , validating our composite approach
315 (**Extended Data Fig. 7i**).
316
317

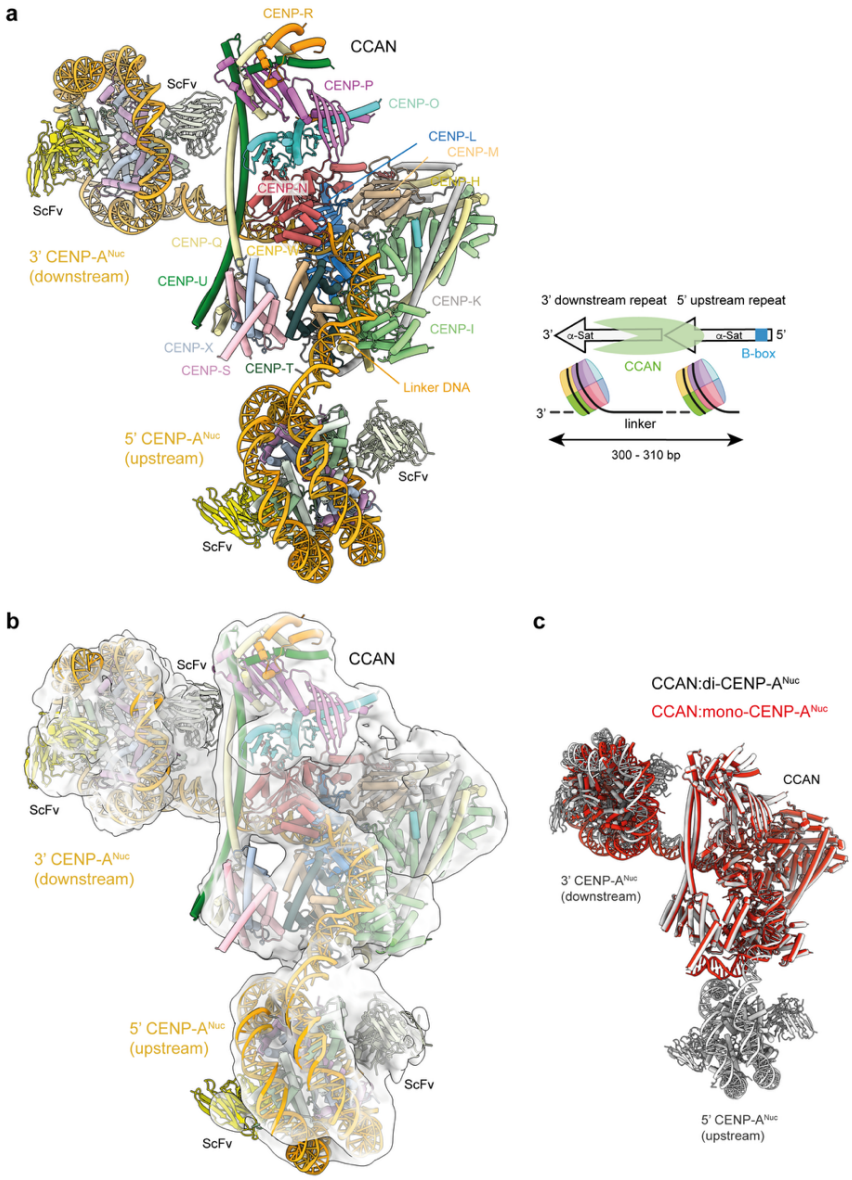

Fig. 4. Structure of the CCAN:di-CENP-A^{Nuc} complex. **a**, Ribbons representation of CCAN:di-CENP-A^{Nuc} complex. Insert: Schematic of the CCAN:di-CENP-A^{Nuc} on a dimer of α-satellite repeats. 20-25 bp of the upstream CENP-A nucleosome is unwrapped. A total of 300-310 bp of DNA is embedded by the complex. A B-box accessible for CENP-B binding in the upstream repeat is shown in blue. **b**, Cryo-EM map of CCAN:di-CENP-A^{Nuc} complex. **C**. Superimposition of the new CCAN:CENP-A^{Nuc} and CCAN:di-CENP-A^{Nuc} complexes showing the identical position of the 3' CENP-A^{Nuc}.

CCAN bound to linker DNA forces DNA unwrapping from CENP-TWSX and 5' CENP-A^{Nuc}

5' CCAN:CENP-A^{Nuc} complex: Despite the limited resolution of this map, reliable alignment of CENP-A^{Nuc} into cryo-EM density was facilitated by the ScFv associated with both sides of the nucleosome (**Fig. 4b**). Analysis of this structure indicated that a CENP-A nucleosome

333 positioned 5' to CCAN is incompatible with DNA wrapping around the CENP-TWSX module
334 (**Fig. 4a, b)**. Analogous to our previous CCAN:CENP-A^{Nuc} and CCAN:DNA complexes [12], we
335 observe that as DNA exits the CCAN-DNA tunnel, it runs along the CENP-I-CENP-TW channel,
336 although unlike our new CCAN:DNA and CCAN:CENP-A^{Nuc} complexes (this study), does not
337 continue to bend around CENP-SX, but instead projects in a straighter trajectory to join the
338 DNA of the 5' CENP-A nucleosome. The DNA gyre of the 5' CENP-A nucleosome connected
339 to linker DNA is itself unwrapped by 20-25 bp. Thus, even without DNA wrapping around
340 CENP-SX, the 5' CENP-A nucleosome is forced to unwrap to allow its positioning onto an
341 upstream α-satellite repeat. Our fitting of the 5' CENP-A^{Nuc} to the cryo-EM density map is
342 consistent with the α-satellite repeat length of 171 bp such that the DNA length from the
343 end of the downstream (3') α-satellite repeat sequence to the dyad axis of the 5' CENP-A^{Nuc}
344 is 74 bp (**Fig. 4a**).
345
346 3' CCAN:CENP-A^{Nuc} complex: The position and orientation of the 3' CENP-A^{Nuc} in the
347 CCAN:di-CENP-A^{Nuc} complex is the same as our new CCAN:mono-CENP-A^{Nuc} complex with
348 211 bp DNA (this study), differing from that in the previously published CCAN:CENP-A^{Nuc}
349 complex [12] (**Fig. 4a, c**). Thus, the ScFv used for the CCAN:di-CENP-A^{Nuc} structure
350 determination does not affect the orientation of the 3' CENP-A^{Nuc}, consistent with modelling
351 showing that ScFv binding to CENP-A^{Nuc}, when in the mono-CENP-A^{Nuc} position, is possible
352 without a steric clash with CCAN.
353
354 **Discussion**
355
356 In this study we investigated the molecular basis for how human CCAN interacts with CENP-
357 A nucleosomes and DNA of α-satellite repeat arrays, revealing that CCAN engages as much
358 as 70 bp of DNA. As described previously [12], DNA threads through the enclosed tunnel
359 generated by the CENP-LN module, CENP-I and CENP-TW subunits. The longer DNA
360 sequences used in this study showed additional DNA interactions with the CENP-SX subunits
361 of the CENP-TWSX HFD module. The CENP-TWSX subunits interact with DNA analogously to
362 how the H3:H4 heterotetramer, in the context of octameric nucleosomes, wraps its DNA
363 gyre. The specific details of the interactions of DNA with CENP-SX, together with CENP-TW,
364 observed in our structure, are in agreement with biochemical and cell biology data,
365 confirming the proposal that human CCAN incorporates a nucleosome-like particle at the
366 centromere [20,32]. Consistent with this, CENP-TWSX augments the affinity of CCAN for a
367 CENP-A nucleosome three-fold [12]. Thus, this study indicates that CCAN creates a tight
368 attachment to centromeric DNA by both topological entrapment of DNA through the CCAN

369 DNA-binding tunnel (CENP-LN, CENP-I), and by wrapping DNA around a HFD tetramer
370 (CENP-TWSX), mimicking the mechanism by which nucleosomes package DNA.
371
372 The finding that CCAN alone engages 65-70 bp of DNA has implications for the higher-order
373 architecture of CCAN and CENP-A nucleosomes on repetitive α-satellite sequences. The 65
374 bp of extranucleosomal DNA bound by CCAN greatly exceeds the 24 bp linker DNA
375 connecting two adjacent and fully wrapped nucleosomes (147 bp) on tandem α-satellite
376 repeats. In our CCAN:CENP-A^{Nuc} structures, 10 bp of DNA are unwrapped from the 3' CENP-
377 A nucleosome gyre as it enters the CCAN DNA-binding tunnel ([12] and this study). Thus, to
378 accommodate 65 bp of DNA interacting with CCAN requires ~30 bp DNA of the upstream α-
379 satellite repeat, in addition to the 24 bp of α-satellite extranucleosomal linker DNA and 10
380 bp of unwrapped DNA from the downstream CENP-A nucleosome (**Fig. 3c**). Since CENP-A
381 nucleosomes are positioned exactly on α-satellite repeats such that the 3' end of the repeat
382 defines the start of the CENP-A nucleosome DNA gyre [12,13], the 30 bp of upstream α-satellite
383 repeat DNA would require the upstream CENP-A nucleosome to unwrap 30 bp of DNA. Such
384 unwrapping is potentially feasible as demonstrated by the extensive levels of DNA
385 unwrapping from CENP-A nucleosomes documented previously [12,16,24,37-42]. To test whether
386 CCAN associates with DNA connecting two adjacent CENP-A nucleosomes, we reconstituted
387 a dimeric α-satellite repeat with CENP-A nucleosomes. SEC and iSCAT data confirmed
388 interactions of CCAN with a dimeric α-satellite repeat with two CENP-A nucleosomes
389 (**Extended Data Fig. 3**). That this interaction required the free linker DNA connecting the
390 two nucleosomes was confirmed by the ability of CCAN to displace CENP-B from its B-box
391 binding site located within the linker DNA (**Extended Data Fig. 4d, e**). Our cryo-EM structure
392 of the CCAN:di-CENP-A^{Nuc} complex revealed CCAN bound to DNA linking two CENP-A
393 nucleosomes (**Fig. 4**). However, accommodating CCAN at this site involved not only 20-25 bp
394 of DNA to be unwrapped from the 5' upstream CENP-A nucleosome, but also dissociation of
395 DNA from CENP-SX. Thus, although the upstream CENP-A nucleosome is unwrapped, the
396 available free DNA duplex is insufficient to bind CENP-SX, presumably because of steric
397 hindrance between the upstream CENP-A nucleosome and CCAN.
398
399 Whether such an arrangement of tandem CENP-A nucleosomes and central CCAN that we
400 observe in our CCAN:di-CENP-A^{Nuc} complex occurs at native human centromeres is unclear.
401 The dissociation of DNA from CENP-SX is inconsistent with the role of conserved basic
402 residues of CENP-SX in binding DNA revealed by our CCAN:DNA and CCAN:mono-CENP-A^{Nuc}
403 structures and from prior *in vitro* binding assays [32]. Furthermore, the extensive unwrapping
404 of DNA from a CENP-A nucleosome, although observed for a small population of particles in
405 a cryo-EM study [42], is not consistent with CENP-A nucleosomes defining a 120 bp footprint *in*

406 *vivo* [13,46], and the size of the nuclease-resistant core observed *in vitro*. Although our cryo-EM
407 structure of the CCAN:di-CENP-A^{Nuc} complex embeds a total of 300-310 bp (**Fig. 4a**), in
408 agreement with the 250-300 bp centromere core-selective footprint identified by single
409 molecule chromatin fibre sequencing (Fiber-seq) [46], we propose two alternative scenarios
410 for the arrangement of CCAN and CENP-A nucleosomes on α-satellite arrays. In one
411 scenario, the kinetochore unit would constitute a monomeric CCAN:CENP-A^{Nuc} complex in
412 which DNA from the upstream α-satellite repeat engages CENP-TWSX such that a total of
413 200-210 bp of DNA is bound by the CCAN:CENP-A^{Nuc} complex (**Fig. 3**). In a second related
414 scenario, a central CENP-A nucleosome would interact with two flanking CCAN protomers in
415 a pseudo-symmetric arrangement of the mono-CCAN:CENP-A^{Nuc} complex (di-CCAN:CENP-
416 A^{Nuc}) (**Fig. 5**). This proposed assembly, with the central CENP-A nucleosome and associated
417 CCAN protomers spanning three α-satellite repeats, embeds 260-270 bp. The 210 bp bound
418 by mono-CCAN:CENP-A^{Nuc} is shorter than the 250-300 bp centromere core-selective
419 footprint [46], however the 260-270 bp bound to the proposed di-CCAN:CENP-A^{Nuc} complexes
420 matches the reported 250-300 bp centromere footprint. We note that Dubocanin et al.,
421 (2025) also identified centromere-associated footprints of 210 bp in size [46]. Although these
422 were assigned as di-nucleosomes, it is also plausible that these methylation-free footprints
423 correspond to mono-CCAN:CENP-A^{Nuc} assemblies. Consistent with this, a recent cryo-ET
424 study of human centromeres found that the majority of putative kinetochore particles were
425 consistent in size with a mono-CCAN complex closely associated with a single CENP-A
426 nucleosome [47]. Additionally, larger globular densities containing multiple nucleosomes and
427 CCAN complexes were also observed, although whether these constitute tandem CCAN and
428 CENP-A^{Nuc} complexes was not defined.
429

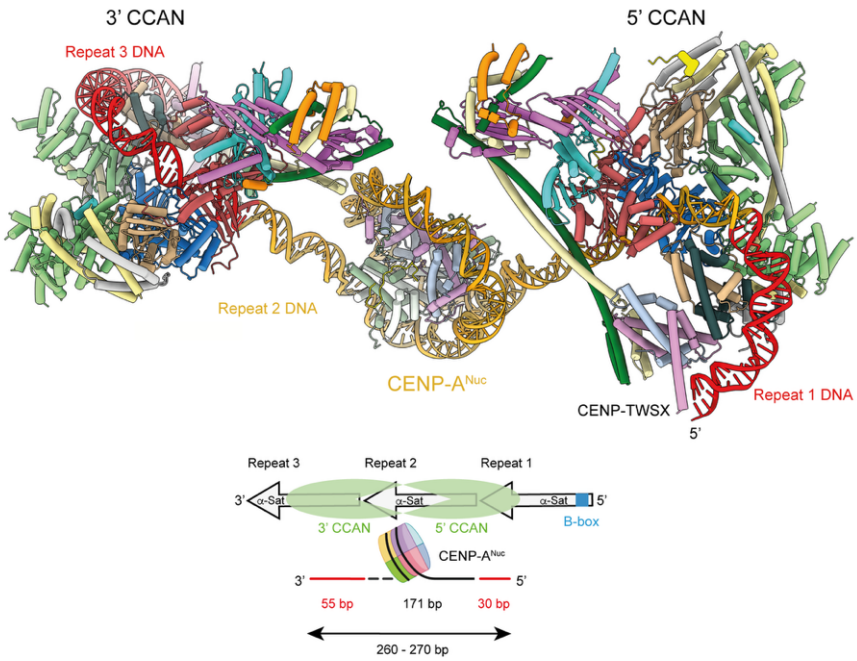

Fig. 5. Model of a di-CCAN:CENP-A^{Nuc} complex. The model was generated from the CCAN:mono-CENP-A^{Nuc} structure by superimposing on CENP-A^{Nuc}. The two CCANs together with a single CENP-A^{Nuc} overlap three α-satellite repeats. In the model, DNA from the central α-satellite sequence is coloured gold. DNA bound to the two CCANs from the 5' and 3' α-satellite repeats (repeats 1 and 3, respectively) is coloured red. Insert: Schematic of the model with DNA coloured red for the 5' and 3' repeats as in the model. A B-box accessible for CENP-B binding in the upstream repeat is shown in blue. B-boxes in the two upstream repeats are occluded by CCAN. 260-270 bp of DNA are bound by the di-CCAN:CENP-A^{Nuc} complex.

Finally, in this study we show that the association of CCAN and CENP-B to the same extranucleosomal linker DNA is mutually exclusive (**Extended Data Fig. 4**). As indicated in Figures 3 to 5, for all three models of CCAN:CENP-A^{Nuc} complexes discussed above, a B-box in the upstream α-satellite repeat is accessible for CENP-B binding.

In summary this work, combined with recent 2D and 3D mapping of CCAN, CENP-A nucleosomes and DNA-binding proteins at native centromeres [46,47], suggest potentially heterogenous structures of CCAN and CENP-A nucleosomes assembled on α-satellite repeat arrays including mono-CCAN:CENP-A^{Nuc}, di-CCAN:CENP-A^{Nuc} and CCAN:di-CENP-A^{Nuc} complexes.

Supplementary Video 1. Video illustrates the difference in position of the 3' CENP-A nucleosome between our previous CCAN:CENP-A^{Nuc} complex with 171 bp DNA (grey cartoon) [12] and the new structure of CCAN:CENP-A^{Nuc} with 211 bp DNA (ASW6) (colour-coded according to subunits as in Fig. 1). Relative to the previous CCAN:CENP-A^{Nuc} structure, in the new model, the DNA register of the α-satellite repeat is shifted 6 bp (translation of 20

Å) away from CCAN (towards the 3' end). Because the DNA phosphate backbone contacts with CCAN are preserved, this results in a 216° rotation of CENP-A^{Nuc}.

Methods

DNA cloning

Protein complexes for CCAN and CENP-A histone octamer were prepared as previously described [12], except CENP-Q was modified to CENP-Q$^{55-268}$, CENP-U was modified to CENP-U$^{235-418}$, CENP-I was changed to isoform 1 from previously isoform 2, and CENP-B full length was cloned into pOPINS plasmid, with a double strep II-sumo-tev tag at their N-termini. The DNA fragment ASW14 was designed as two repeats from α-satellite DNA of chromosome 2 with 91 base pairs centred on their dyad positions replaced with Widom601 sequence aligned at the dyad base. A B-box sequence is in the linker region. Six ASW14 fragments flanked by GATATC (EcoRV recognition site) were assembled into the pMK-RQ plasmid. The plasmid containing ASW14 fragments was produced by using Plasmid Plus Giga Kit (QIAGEN). The DNA fragment was released by EcoRV-HF (NEB) at 37C over night. The digested sample was diluted five-fold with PBS and loaded onto a pre-equlibrated (PBS) 1 mL Resource Q Column (GE 17-1177-01, Merck). The column was washed with 10 mL PBS (buffer A), followed by a wash with 20 mL of 50% of buffer B (PBS with 850 mM NaCl). The DNA fragment was eluted using a gradient to 70% of buffer B at 1 mL.min^{-1} over 120 min. The target fragment eluted around 60% buffer B. The fractions containing DNA were checked on an agarose gel, and DNA was precipitated using 1:1 of isopropanol at 20 °C for 30 min at 15,000g. The DNA pellet was dissolved in the buffer needed for its following application.

The sequence of the generated ASW14 fragment is:

```
1      ATCAGGAAAT ATCTTCACAT AAAAACTAGA CAATTGGTCG TAGACAGCTC TAGCACCGCT
61     TAAACGCACG TACGCGCTGT CCCCCGCGTT TTAACCGCCA AGGGGATTAC TCCCTAGTCT
121    CCTTGTAGTA TCTGCAAGTG GACATTCGGA GCACTTTGTG GCCTTCGTTG GAAACGGGAA
181    TATGTTCACA TAAAAACTAG ACAATTGGTC GTAGACAGCT CTAGCACCGC TTAAACGCAC
241    GTACGCGCTG TCCCCCGCGT TTTAACCGCC AAGGGGATTA CTCCCTAGTC TCCTTGTAGT
301    ATCTGGAATT GGACATTTGG AGAT
```

The Widom601 sequence underlined. Dyad base of the two CENP-A^{Nuc} indicated in italics. ASW14 with mutant B-box: The B-box of CTTCGTTGGAAACGGGA in bold of ASW14 was mutated to CAAAATTGGTAATTTTA in the B-box mutant α-satelitte repeat dimer.

494 The 211 bp DNA fragment for the CCAN:CENP-A^{Nuc} complex (ASW6) has an additional 40 bp
495 5' of an α-satellite repeat sequence (AS2) with a central 92 bp Widom601 sequence. ASW6
496 sequence is:
497
498 1 CATACTCTTT TTGTAGTATC TGCAAGTGGA CATTCGGAGC ACTTTGTGGC CTTCGTTGGA
499 61 AACGGGAATA TGTTCACATA AAAACTAGAC AATTGGTCGT AGACAGCTCT AGCACCGCTT
500 121 AAACGCACGT ACGCGCTGTC CCCCGCGTTT TAACCGCCAA GGGGATTACT CCCTAGTCTC
501 181 CTTGTAGTAT CTGGAATTGG ACATTTGGAG AT
502
503 CCAN:DNA complex assembly
504
505 CCAN:DNA complexes were assembled in CCAN buffer (300 mM NaCl, 20 mM Hepes pH 7.8,
506 0.5 mM TCEP) as follows. 6 µM CCAN was incubated at 22 °C for 30 mins before addition of
507 an equal volume of 6 µM 171 bp (α-satellite repeat) DNA (AS2 described in [12]), and
508 incubated for a further 30 mins at at 22 °C, resulting in a final CCAN:DNA concentration of 3
509 µM and a final volume of 100 µL. The CCAN:DNA complex was then centrifuged at 10 °C in a
510 table-top centrifuge for 10 min. To stabilize complexes for cryo-EM analysis, on-column
511 crosslinking was performed.
512
513 On-column crosslinking of CCAN:DNA
514
515 An Agilent 500 column coupled to a MicroAkta was pre-equilibrated in CCAN buffer. 100 µL
516 2.5 mM BS(PEG)$_5$ (ThermoFisherScientific) was injected into the system for 1 mL at a flow
517 rate of 0.07 µL/min. The CCAN:DNA complex was then injected into the column and eluted
518 at the same flow rate into a 96-well plate in 50 µL fractions. Each plate well was
519 supplemented with 5 µL 1 M Tris.HCl buffer pH 7.4 to quench the crosslinker during elution.
520 Fractions containing CCAN:DNA were pooled, buffer exchanged into 150 mM NaCl, 20 mM
521 Hepes pH 7.8, 0.5 mM TCEP and concentrated to 1.5 mg.mL^{-1} (Amicon 100 kDa, 0.5 mL).
522 Following concentration, CCAN:DNA complexes were again centrifuged at 10 °C in a table-
523 top centrifuge for 10 min.
524
525 CENP-A mono-nucleosome (ASW6) and CENP-A di-nucleosome (ASW14) reconstitution
526
527 The CENP-A histone octamer was prepared as described previously [12]. Either ASW6 or
528 ASW14 DNA were desalted into buffer B (20 mM HEPES pH 7.5, 2 M KCl). DNA at 8 µM was
529 mixed with the CENP-A histone octamer at molar ratios of 1.1:1 protein:DNA for mono-
530 CENP-A^{Nuc} and 2.1:1 protein:DNA for di-CENP-A^{Nuc}. The histone octamers were then wrapped
531 with DNA using the gradient dialysis method starting from 2 M KCl (in 20 mM HEPES pH 7.5,
532 1 mM EDTA) to 300 mM KCl over 16 h at 22 °C. The mixture was then dialysed against 20
533 mM HEPES pH 7.5, 300 mM KCl, 1 mM EDTA for a further 5 h. The wrapped mono-CENP-A
534 and di-CENP-A nucleosomes were assessed by agarose gel and stored at 4 °C.

535

536 Assembly of the CCAN:CENP-A^{Nuc} (ASW6 DNA) complex

537

538 CENP-A^{Nuc} and CCAN components (CENP-C^{N}, CENP-LN, CENP-HIKM, CENP-TWSX, and CENP-
539 OPQUR$^{\Delta N}$) were mixed at a 1:1 molar ratio at 5 μM in PBS buffer and TCEP. The sample was
540 injected into an Agilent Bio SEC-5 1000A 4.6x300 column in CCAN gel filtration buffer (20
541 mM HEPES pH 7.8, 300 mM NaCl, 1 mM TCEP). The peak fractions were analysed using a 4-
542 12% SDS-PAGE gel, stained with Instant Blue Coomassie Stain. To prepare the complex for
543 structural analysis, on-column cross-linking using BS(PEG)$_5$ (ThermoFisherScientific) was
544 performed. 100 µl of 2.5 mM BS(PEG)$_5$ was injected into an Agilent Bio SEC-5 1000A 4.6x300
545 column (equilbrated in PBS buffer) at a flow rate set of 0.07 µL/min, then 0.2 mL buffer, after
546 which the CCAN:CENP-A^{Nuc} sample in (100 µl) was applied and eluted in PBS buffer. The
547 sample was eluted into a 96-well plate in 50 μL fractions. Each plate well was supplemented
548 with 5 µL 1 M Tris.HCl buffer pH 7.4 to quench the crosslinker during elution. The peak
549 fractions of the CCAN:CENP-A^{Nuc} samples were pooled and concentrated to 1.5 mg.mL^{-1} for
550 cryo-EM grid preparation.

551

552 Assembly of the CCAN:di-CENP-A^{Nuc} (ASW14 DNA) complex

553

554 For assembly of the CCAN:di-CENP-A^{Nuc} (ASW14 DNA) complex, we used the same
555 procedure as for the CCAN:mono-CENP-A^{Nuc} (ASW6 DNA) complex except we used 20 mM
556 HEPES pH 7.8, 300 mM NaCl, 1 mM TCEP buffer in the cross-linking final gel filtration step.

557

558 Assembly of the CCAN$^{\Delta CENP\text{-}C}$:di-CENP-A^{Nuc} (ScFv) (ASW14 DNA) complex

559

560 1. *Cross-linking di-CENP-A^{Nuc} and ScFv (di-CENP-A^{Nuc}:ScFv)*

561 Di-CENP-A^{Nuc} and ScFv were combined at a 1:2.3 molar ratio and dialysed into a buffer of 20
562 mM HEPES pH 7.5, 50 mM NaCl. Cross-linking of the di-CENP-A^{Nuc}:ScFv complex was
563 performed using a 24 mL Superose 6 column by injecting 500 μL of 2.5 mM BS(PEG)$_5$ at a
564 flow rate of 0.25 mL.min^{-1} for 7 mL before loading the CENP-A^{Nuc}:ScFv complex onto the
565 column at the same flow rate. The cross-linking was assessed using SDS-PAGE gel. The cross-
566 linked fractions were pooled and concentrated to 10 μM.

567

568 2. *Assembly of cross-linked di-CENP-A^{Nuc}:ScFv with CCAN*

569 All CCAN components (omitting CENP-C^{N}) were without DTT. The components were at a
570 1:1:1:1:1 molar ratio (CENP-OPQUR:CENP-LN:CENP-HIKM:CENP-TWSX:di-CENP-A^{Nuc}:ScFv)
571 with CCAN components at a concentration of 5 μM. The resultant complex was cross-linked

572 on an Agilent Bio SEC-5 1000A 4.6x300 column. Collected fractions were concentrated to
573 1.5-2 mg.mL^{-1} for cryo-EM grid preparation.
574
575 CCAN displaces CENP-B from di-CENP-A^{Nuc}-B-box
576
577 *Di-CENP-A^{Nuc}-CENP-B binding test*. Di-CENP-A^{Nuc} and CENP-B were mixed at a 1:1 ratio at 5
578 μM final concentration and injected into a Superose 6 Increase 10/300 column (Cytiva).
579 Appropriate fractions were collected and concentrated.
580
581 *Di-CENP-A^{Nuc}-CENP-B-CCAN binding test*. An equal molar ratio of CCAN$^{\Delta CENP-C}$ components
582 (CENP-LN, CENP-HIKM, CENP-TWSX, and CENP-OPQUR$^{\Delta N}$) was added to the di-CENP-
583 A^{Nuc}:CENP-B complex at a final concentration of 5 μM and then loaded onto an Agilent Bio
584 SEC-5 1000A 4.6x300 column. The eluted fractions were visualized using a 4-12% SDS-PAGE
585 gel, stained with InstantBlue Coomassie Stain.
586
587 Mass photometry
588 To assess the oligomeric state of CCAN:di-CENP-A^{Nuc} and CCAN$^{\Delta CENP-C}$:di-CENP-A^{Nuc}, 18 μL of
589 sample at approximately 100 nM was applied to wells in silicone gaskets on clean coverslips
590 (Refeyn, UK) on a OneMP instrument (Refeyn). Movies were imaged for 60 s using the
591 AcquireMP software (Refeyn) and the results were processed using the DiscoverMP
592 software. The data were analysed by using automatic Gaussian fitting. The contrast
593 intensities of landing events due to interference scattering were converted to masses using a
594 calibration performed with a standard set of protein oligomers (P1, Refeyn) under similar
595 buffer conditions. Data events were exported and plotted in Prism (GraphPad).
596
597 Cryo-EM grid preparation and data collection
598
599 *CCAN:DNA sample vitrification*
600 Immediately prior to plunge-freezing, CCAN:DNA samples were supplemented with n-octyl-
601 β-D-glucopyranoside (Glycon-biochem) to a final concentration of 0.05%. Quantifoil 300
602 mesh copper R1.2/1.3 grids (Quantifoil Micro Tools) were rendered hydrophilic by glow
603 discharge in a Edwards S150B glow discharger for 1 min 15 sec, setting 6, 30-35 mA, 1.2 kV,
604 0.2 mBar (0.15 Torr). Subsequently, 3 μL sample was applied to the grids, which were then
605 mounted in a Vitrobot IV (Thermo Fisher Scientific), blotted with Whatman Filter paper 1 (0-
606 0.5 s waiting time, 2 s blotting time, -7 blotting force), and plunge frozen in liquid ethane
607 maintained at a temperature of -170 °C.
608
609 *CCAN:DNA data aquisition*

610 10,628 micrograph movies were collected on a Titan Krios (ThermoFisherScientific) electron
611 microscope, equipped with a K3 direct electron detector (Gatan) and energy filter (Gatan)
612 with a slit width of 20 eV, operating at 300 keV with a flux of 25 e^-/pixel/s, at a nominal
613 magnification of 105k, yielding a pixel size of 0.725 Å/px and a total dose of 40e/$Å^2$.
614 Automated data acquisition was performed using EPU (ThermoFisherScientific) with
615 aberration-free image shift enabled, and a defocus range of -0.8 to -2.2 µm in 0.2 µm
616 increments.
617
618 *CCAN:CENP-A^{Nuc} complex sample vitrification and cryo-EM data acquistion*
619 To prepare the CCAN:CENP-A^{Nuc} complex for cryo-EM, 3.5 µL of sample at a concentration of
620 2 $mg.mL^{-1}$ was applied to glow-discharged Quantifoil R2/1 300 mesh copper grids (Quantifoil
621 Micro Tools). Grids were blotted for 2 s at 4°C , 100% humidity, and a blotting force of -10,
622 then plunge-frozen in liquid ethane using a Vitrobot Mark IV (Thermo Fisher Scientific). Data
623 were collected on a Titan Krios microscope (Thermo Fisher Scientific) operated at 300 kV,
624 equipped with a K3 direct electron detector (Gatan) and an energy filter (Gatan) with an
625 energy slit of 20 eV. Images were acquired at a nominal magnification of 81,000×,
626 corresponding to a pixel size of 1.072 Å. Movies were recorded at a dose rate of 15 e^-/pixel/s
627 with an exposure time of 3 s over 40 frames. Automated data collection was performed
628 using EPU (Thermo Fisher Scientific) with aberration-free image shift (AFIS) enabled. The
629 defocus range was set from -1.0 to -2.0 µm in 0.2 µm increments. A total of 50,781 movie
630 frames were collected.
631
632 *CCAN:di-CENP-A^{Nuc} complex sample vitrification and cryo-EM data acquistion*
633 To prepare the CCAN:di-CENP-A^{Nuc} complex for cryo-EM, 3.5 µL of sample at a concentration
634 of 2 $mg.mL^{-1}$ was applied to glow-discharged Quantifoil R1.2/1.3 300 mesh copper grids
635 (Quantifoil Micro Tools). Grids were blotted for 2 s at 4°C , 100% humidity, and a blotting
636 force of -7, then plunge-frozen in liquid ethane using a Vitrobot Mark IV (Thermo Fisher
637 Scientific). Data were collected on a Titan Krios microscope (Thermo Fisher Scientific)
638 operated at 300 kV, equipped with a K3 direct electron detector (Gatan) and an energy filter
639 (Gatan) with an energy slit of 20 eV. Images were acquired at a nominal magnification of
640 81,000×, corresponding to a pixel size of 0.928 Å. Movies were recorded at a dose rate of
641 25 e^-/pixel/s with an exposure time of 1.3 s over 82 frames. Automated data collection was
642 performed using EPU (Thermo Fisher Scientific) with aberration-free image shift (AFIS)
643 enabled. The defocus range was set from -1.0 to -2.0 µm in 0.2 µm increments. A total of
644 28,703 movie frames were collected.
645
646 <u>Cryo-EM data processing</u>

647

648 *CCAN:DNA complex*

649 Micrograph movies were imported into RELION [45] and motion-corrected using RELION's own
650 implementation of MotionCor2 [48], followed by contrast transfer function estimation using
651 the RELION wrapper for CTFFIND4 [49]. Particle picking was performed using the crYOLO
652 general model and particles were extracted in RELION with a box size of 150 pixels. Particles
653 were subsequently exported to cryoSPARC and subjected to 2D classification. Particles
654 exhibiting clear secondary structure features were used to generate an *ab initio*
655 reconstruction. The initial particle set was then subjected to three rounds of heterogeneous
656 refinement against one true volume (the CCAN:DNA *ab initio* reconstruction) and three
657 noise decoy volumes arising from *ab initio* reconstruction of particles with no obvious
658 proteo-typic features. Particles accumulating in the CCAN:DNA class were selected for each
659 subsequent round of refinement until few or no particles reclassified into the noise decoy
660 classes. The cleaned particle set was then subjected to homogeneous refinement, followed
661 by 3D variability analysis. Particles exhibiting the most continuous DNA and CCAN subunit
662 density were re-extracted without binning in RELION and subjected to particle polishing and
663 CTF refinement. Finally, polished and CTF-corrected particles were re-imported into
664 cryoSPARC where a final round of homogeneous refinement was performed, yielding a 3D
665 reconstruction of CCAN:DNA to an overall resolution of 3.54 Å. The resulting map was
666 filtered according to local resolution, as estimated in cryoSPARC, and then used for structural
667 model building (in COOT) [50] and real-space refinement in PHENIX [51].

668

669 *CCAN:CENP-A^{Nuc} complex*

670 For the CCAN:CENP-A^{Nuc} complex, movie frames were motion-corrected, followed by
671 estimation of Contrast transfer function (CTF) parameters using the patch-based method in
672 cryoSPARC [52]. Particle picking was performed with crYOLO [53] using the genaral model, and
673 particles were extracted with a box size of 400 pixels. Reference-free 2D classfication was
674 then conducted to clean the particle dataset. Classes exhibting clear secondary structure
675 features were selected for *ab-initio* reconstruction and heterogeneous refinement in
676 cryoSPARC. One class with 1,525,520 particles showing nucleosome features was selected
677 for non-uniform refinement, yielding a reconstruction of the CENP-A^{Nuc}:CENP-C^{N} at 2.4 Å
678 resolution. Another dominant classs containing 3,815,026 particles was import into RELION
679 for further 3D classification. Three classes displaying CCAN feature were selected for particle
680 subtraction using a mask covering 3' CENP-A^{Nuc} region. After an additional round of 2D and
681 3D classifion on the recentered particle dataset, 325,201 well-aligned nucleosome particles
682 were reverted to their original, un-subtracted particles for further 3D classification. This

683 yielded a subset of 39,036 particles corresponding to the CENP-A^{Nuc}:CCAN complex, which
684 was refined to 4.5 Å resolution using Refine3D followed by Post-process.
685
686 *CCAN:di-CENP-A^{Nuc} complex*
687 For the CCAN:di-CENP-A^{Nuc} complex, all movie frames were motion-corrected, followed by
688 estimation of Contrast transfer function (CTF) parameters using the patch-based method in
689 cryoSPARC. Particle picking was performed with crYOLO using the genaral model, and the
690 particles were extracted with a box size of 400 pixels. Reference-free 2D classfication was
691 then conducted to clean the particle dataset, and classes exhibting clear secondary structure
692 features were selected for *ab-initio* reconstruction and heterogeneous refinement in
693 cryoSPARC. Three well-populated classes with clear structural features were further selected
694 for non-uniform refinement, CTF refinement and local refinement, resulting three high-
695 resolution maps: CENP-A^{Nuc}:ScFv (1:1), CENP-A^{Nuc}:ScFv (1:2) and CCAN:DNA, resolved at 2.7
696 Å, 2.7 Å and 2.9 Å, respectively.
697
698 To dissect the CENP-A^{Nuc} association with CCAN, the CCAN:DNA data was exported to
699 RELION [45] for 3D classification, which revealed diffuse density at both the 3' and 5' end of
700 the DNA. To recover CENP-A^{Nuc} at each side, two masks were genarated and to subtract the
701 density outside either the 3' or 5' CENP-A^{Nuc} regions. After re-centering the particle on the 3'
702 or 5' CENP-A^{Nuc}, nucleosome density was resolved at both side, as confirmed by 2D
703 classfication and 3D classfication showing dominant classes with clear nucleosome views.
704 These dominant classes were reverted to their original un-subtracted particles for further 3D
705 classification, yielding two subsets: 9,661 particles of CCAN:3' CENP-A^{Nuc} and 5,396 particles
706 of CCAN:5' CENP-A^{Nuc}. These were refined to 9.5 Å and 15.5 Å respectively. Subsequent
707 multibody refinement and post-process modestly improved the map quality of both the
708 CCAN:DNA and CENP-A^{Nuc} modules. Finally, the maps of CCAN with 3' and 5' CENP-A^{Nuc},
709 were combined to gerarate a composite map of the CCAN di-CENP-A^{Nuc} complex.
710
711 <u>Cryo-EM model building and refinement</u>
712
713 For the CCAN:DNA structure, the PDB entry 7R5S was used as the initial model. The model
714 was fitted into the cryo-EM map of CCAN:DNA, and the DNA wrapping around CENP-
715 TWSX was guided by a predicted CCAN:DNA model generated using AlphaFold3, followed
716 by manual correction in COOT and real-space refinement in PHENIX. For the CCAN:CENP-A^{Nuc}
717 structure, the newly refined CCAN:DNA complex model was docked into the corresponding
718 map, followed by docking of a 3' CENP-A^{Nuc} using PDB entry 7YWX. The models were then
719 combined in COOT and real-space refined in PHENIX. For the CCAN:di-CENP-A^{Nuc} model,

a composite map combining CCAN:3' CENP-A^{Nuc} and CCAN:5' CENP-A^{Nuc} was used. The CCAN:DNA model was first fitted into the map, followed by docking of CENP-A^{Nuc} models (PDB: 6E0P) to the 3' and 5' nucleosomes, respectively. All models were then combined in COOT, and the linker DNA region was manually built and refined. Additional manual corrections were also performed in COOT. Figures were generated using ChimeraX [54].

Data availability

Atomic models and cryo-EM maps have been deposited in the Protein Data Bank and the Electron Microscopy Data Bank, respectively. Accession numbers are listed in Extended Data Table 1.

Acknowledgements

We are grateful to the LMB and eBIC EM Facilities for help with the EM data collection; J. Grimmett, T. Darling and I. Clayson for scientific computing; K. Turton for help with insect cell expression. We thank Andrea Musacchio, Marion Pesenti and Ingrid Vetter for sharing unpublished experimental observations. For the purpose of open access, the authors have applied a CC BY public copyright license to any Author Accepted Manuscript version arising.

Funding

UKRI/Medical Research Council MC_UP_1201/6 (D.B.)

Cancer Research UK C576/A25675 (D.B.)

References

1. Ariyoshi, M. & Fukagawa, T. An updated view of the kinetochore architecture. *Trends Genet* **39**, 941–953 (2023).
2. McAinsh, A.D. & Marston, A.L. The Four Causes: The Functional Architecture of Centromeres and Kinetochores. *Annu Rev Genet* **56**, 279–314 (2022).
3. Musacchio, A. & Desai, A. A Molecular View of Kinetochore Assembly and Function. *Biology (Basel)* **6**(2017).
4. McAinsh, A.D. & Kops, G. Principles and dynamics of spindle assembly checkpoint signalling. *Nat Rev Mol Cell Biol* **24**, 543–559 (2023).
5. Fischer, E.S. Kinetochore-catalyzed MCC formation: A structural perspective. *IUBMB Life* **75**, 289–310 (2023).
6. Altemose, N. et al. Complete genomic and epigenetic maps of human centromeres. *Science* **376**, eabl4178 (2022).
7. Bodor, D.L. et al. The quantitative architecture of centromeric chromatin. *Elife* **3**, e02137 (2014).
8. Logsdon, G.A. et al. The structure, function and evolution of a complete human chromosome 8. *Nature* **593**, 101–107 (2021).

762 9. Gershman, A. et al. Epigenetic patterns in a complete human genome. *Science* **376**,
763 eabj5089 (2022).
764 10. Blower, M.D., Sullivan, B.A. & Karpen, G.H. Conserved organization of centromeric
765 chromatin in flies and humans. *Dev Cell* **2**, 319–30 (2002).
766 11. Luger, K., Mader, A.W., Richmond, R.K., Sargent, D.F. & Richmond, T.J. Crystal
767 structure of the nucleosome core particle at 2.8 A resolution. *Nature* **389**, 251–60
768 (1997).
769 12. Yatskevich, S. et al. Structure of the human inner kinetochore bound to a centromeric
770 CENP-A nucleosome. *Science* **376**, 844–852 (2022).
771 13. Hasson, D. et al. The octamer is the major form of CENP-A nucleosomes at human
772 centromeres. *Nat Struct Mol Biol* **20**, 687–95 (2013).
773 14. Corda, L. & Giunta, S. Chromosome-specific centromeric patterns define the centeny
774 map of the human genome. *Science* **389**, eads3484 (2025).
775 15. Fujita, R. et al. Stable complex formation of CENP-B with the CENP-A nucleosome.
776 *Nucleic Acids Res* **43**, 4909–22 (2015).
777 16. Nagpal, H. et al. CENP-A and CENP-B collaborate to create an open centromeric
778 chromatin state. *Nat Commun* **14**, 8227 (2023).
779 17. Chardon, F. et al. CENP-B-mediated DNA loops regulate activity and stability of
780 human centromeres. *Mol Cell* **82**, 1751–1767 e8 (2022).
781 18. Magidson, V. et al. Adaptive changes in the kinetochore architecture facilitate proper
782 spindle assembly. *Nat Cell Biol* **17**, 1134–44 (2015).
783 19. Yatskevich, S., Barford, D. & Muir, K.W. Conserved and divergent mechanisms of inner
784 kinetochore assembly onto centromeric chromatin. *Curr Opin Struct Biol* **81**, 102638
785 (2023).
786 20. Hori, T. et al. CCAN makes multiple contacts with centromeric DNA to provide distinct
787 pathways to the outer kinetochore. *Cell* **135**, 1039–52 (2008).
788 21. Pesenti, M.E. et al. Structure of the human inner kinetochore CCAN complex and its
789 significance for human centromere organization. *Mol Cell* **82**, 2113–2131 e8 (2022).
790 22. Dendooven, T. et al. Cryo-EM structure of the complete inner kinetochore of the
791 budding yeast point centromere. *Sci Adv* **9**, eadg7480 (2023).
792 23. Tian, T. et al. Structural insights into human CCAN complex assembled onto DNA. *Cell*
793 *Discov* **8**, 90 (2022).
794 24. Yan, K. et al. Structure of the inner kinetochore CCAN complex assembled onto a
795 centromeric nucleosome. *Nature* **574**, 278–282 (2019).
796 25. Hinshaw, S.M. & Harrison, S.C. The structure of the Ctf19c/CCAN from budding yeast.
797 *Elife* **8**(2019).
798 26. Yu, C.W.H. et al. Architecture and Function of Holocentric CENP-A-Independent
799 Kinetochores. *BioRxiv* (2025).
800 27. Kato, H. et al. A conserved mechanism for centromeric nucleosome recognition by
801 centromere protein CENP-C. *Science* **340**, 1110–3 (2013).
802 28. Klare, K. et al. CENP-C is a blueprint for constitutive centromere-associated network
803 assembly within human kinetochores. *J Cell Biol* **210**, 11–22 (2015).
804 29. McKinley, K.L. et al. The CENP-L-N Complex Forms a Critical Node in an Integrated
805 Meshwork of Interactions at the Centromere-Kinetochore Interface. *Mol Cell* **60**,
806 886–98 (2015).
807 30. Pentakota, S. et al. Decoding the centromeric nucleosome through CENP-N. *Elife*
808 **6**(2017).

31. Walstein, K. et al. Assembly principles and stoichiometry of a complete human kinetochore module. *Sci Adv* **7**(2021).
32. Nishino, T. et al. CENP-T-W-S-X forms a unique centromeric chromatin structure with a histone-like fold. *Cell* **148**, 487–501 (2012).
33. Waterhouse, A.M., Procter, J.B., Martin, D.M., Clamp, M. & Barton, G.J. Jalview Version 2--a multiple sequence alignment editor and analysis workbench. *Bioinformatics* **25**, 1189–91 (2009).
34. Zhao, Q. et al. The MHF complex senses branched DNA by binding a pair of crossover DNA duplexes. *Nat Commun* **5**, 2987 (2014).
35. Dechassa, M.L. et al. Structure and Scm3-mediated assembly of budding yeast centromeric nucleosomes. *Nat Commun* **2**, 313 (2011).
36. Kingston, I.J., Yung, J.S. & Singleton, M.R. Biophysical characterization of the centromere-specific nucleosome from budding yeast. *J Biol Chem* **286**, 4021–6 (2011).
37. Migl, D. et al. Cryoelectron Microscopy Structure of a Yeast Centromeric Nucleosome at 2.7 A Resolution. *Structure* **28**, 363–370 e3 (2020).
38. Tachiwana, H. et al. Crystal structure of the human centromeric nucleosome containing CENP-A. *Nature* **476**, 232–5 (2011).
39. Ariyoshi, M. et al. Cryo-EM structure of the CENP-A nucleosome in complex with phosphorylated CENP-C. *EMBO J* **40**, e105671 (2021).
40. Zhou, B.R. et al. Atomic resolution cryo-EM structure of a native-like CENP-A nucleosome aided by an antibody fragment. *Nat Commun* **10**, 2301 (2019).
41. Roulland, Y. et al. The Flexible Ends of CENP-A Nucleosome Are Required for Mitotic Fidelity. *Mol Cell* **63**, 674–685 (2016).
42. Boopathi, R. et al. Phase-plate cryo-EM structure of the Widom 601 CENP-A nucleosome core particle reveals differential flexibility of the DNA ends. *Nucleic Acids Res* **48**, 5735–5748 (2020).
43. Falk, S.J. et al. Chromosomes. CENP-C reshapes and stabilizes CENP-A nucleosomes at the centromere. *Science* **348**, 699–703 (2015).
44. Ali-Ahmad, A., Bilokapic, S., Schafer, I.B., Halic, M. & Sekulic, N. CENP-C unwraps the human CENP-A nucleosome through the H2A C-terminal tail. *EMBO Rep* **20**, e48913 (2019).
45. Kimanius, D., Dong, L., Sharov, G., Nakane, T. & Scheres, S.H.W. New tools for automated cryo-EM single-particle analysis in RELION-4.0. *Biochem J* **478**, 4169–4185 (2021).
46. Dubocanin, D. et al. Conservation of dichromatin organization along regional centromeres. *Cell Genom* **5**, 100819 (2025).
47. Kixmoeller, K., Tarasovetc, E.V., Mer, E., Chang, Y.W. & Black, B.E. Centromeric chromatin clearings demarcate the site of kinetochore formation. *Cell* **188**, 1280–1296 e19 (2025).
48. Zheng, S.Q. et al. MotionCor2: anisotropic correction of beam-induced motion for improved cryo-electron microscopy. *Nat Methods* **14**, 331–332 (2017).
49. Rohou, A. & Grigorieff, N. CTFFIND4: Fast and accurate defocus estimation from electron micrographs. *J Struct Biol* **192**, 216–21 (2015).
50. Emsley, P., Lohkamp, B., Scott, W.G. & Cowtan, K. Features and development of Coot. *Acta Crystallogr D Biol Crystallogr* **66**, 486–501 (2010).

855 51. Afonine, P.V. et al. Towards automated crystallographic structure refinement with
856 phenix.refine. *Acta Crystallogr D Biol Crystallogr* **68**, 352–67 (2012).
857 52. Punjani, A., Zhang, H. & Fleet, D.J. Non-uniform refinement: adaptive regularization
858 improves single-particle cryo-EM reconstruction. *Nat Methods* **17**, 1214–1221
859 (2020).
860 53. Wagner, T. et al. SPHIRE-crYOLO is a fast and accurate fully automated particle picker
861 for cryo-EM. *Commun Biol* **2**, 218 (2019).
862 54. Goddard, T.D. et al. UCSF ChimeraX: Meeting modern challenges in visualization and
863 analysis. *Protein Sci* **27**, 14–25 (2018).
864

Extended Data Table 1. Cryo-EM data collection, refinement, and validation statistics

Complex	CCAN:DNA PDB XXXX EMD-XXXXX	CCAN:mono-CENP-A PDB XXXX EMD-XXXXX	CCAN:di-CENP-A PDB XXXX EMD-XXXXX	
Data collection and Processing				
Microscope	Titan Krios	Titan Krios	Titan Krios	Titan Krios
Voltage (keV)	300	300	300	300
Camera	K3	K3	K3	K3
Magnification	105,000	81,000	81,000	81,000
Pixel size at detector (Å/pixel)	0.725	1.072	0.928	0.928
Total electron exposure (e^{-}/Å^2)	40	40	40	40
Exposure rate (e-/pixel/sec)	25	15	18	18
Number of frames	40	40	82	82
Defocus range (μm)	0.8-2.2	1-2	1.0-2.0	1.0-2.0
Automation software	EPU	EPU	EPU	EPU
Energy filter slit width (eV)	20	20	20	20
Micrographs collected (no.)	10,628	50,781	28,703	28,703
Total extracted particles (no.)	1,963,587	21,223,394	8,973,622	8,973,622
For each reconstruction:			CCAN/3'-CENP-A	CCAN/5'-CENP-A
Final particles (no.)	80,236	39,306	9,661	5,396
Point-group	C1	C1	C1	C1
Resolution (global, Å)	3.54	4.5	9.5	15.5
Resolution range (local, Å)	3.54-20	4.5-18	9.5-20	15.5-20
Map sharpening *B* factor (Å^2)	-73	-20	-50	-50
Map sharpening methods	cryoSPARC	RELION5	RELION5	RELION5
Model composition				
Protein (residues)	3,165	3,962	5,600	
RNA/DNA (nucleotides)	162	398	636	
Refinement				
Refinement package	PHENIX 1.20.1	PHENIX 1.20.1	PHENIX 1.21	
real or reciprocal space	real	real	real	
Initial model used (Alphafold2)	7R5S/AlphaFold3	7YWX	7R5S/6E0P	
Model-Map scores				
CC Volume/Mask	0.66/0.67	0.48/0.46	0.26/0.36	
B factors (Å^2)				
Protein residues	2.50/63.61/30.63	111.54	80.43	
RNA/DNA	46.81/99.32/79.68	48.18	50	
R.m.s. deviations from ideal values				
Bond lengths (Å)	0.006	0.012	0.012	
Bond angles (°)	1.003	1.160	1.203	
Validation				
MolProbity score	1.56	1.94	1.59	
CaBLAM outliers	1.22	1.38	0.04	
Clashscore	7.26	20.98	6.74	
Poor rotamers (%)	0.14	0	0.29	
C-beta deviations	0	0	0	
EMRinger score	1.26	0.25	*n.d.	
Ramachandran plot				
Favored (%)	97.13	97.37	96.63	
Allowed (%)	2.81	2.48	3.25	
Outliers (%)	0.06	0.15	0.13	

*Not determined (n.d.)

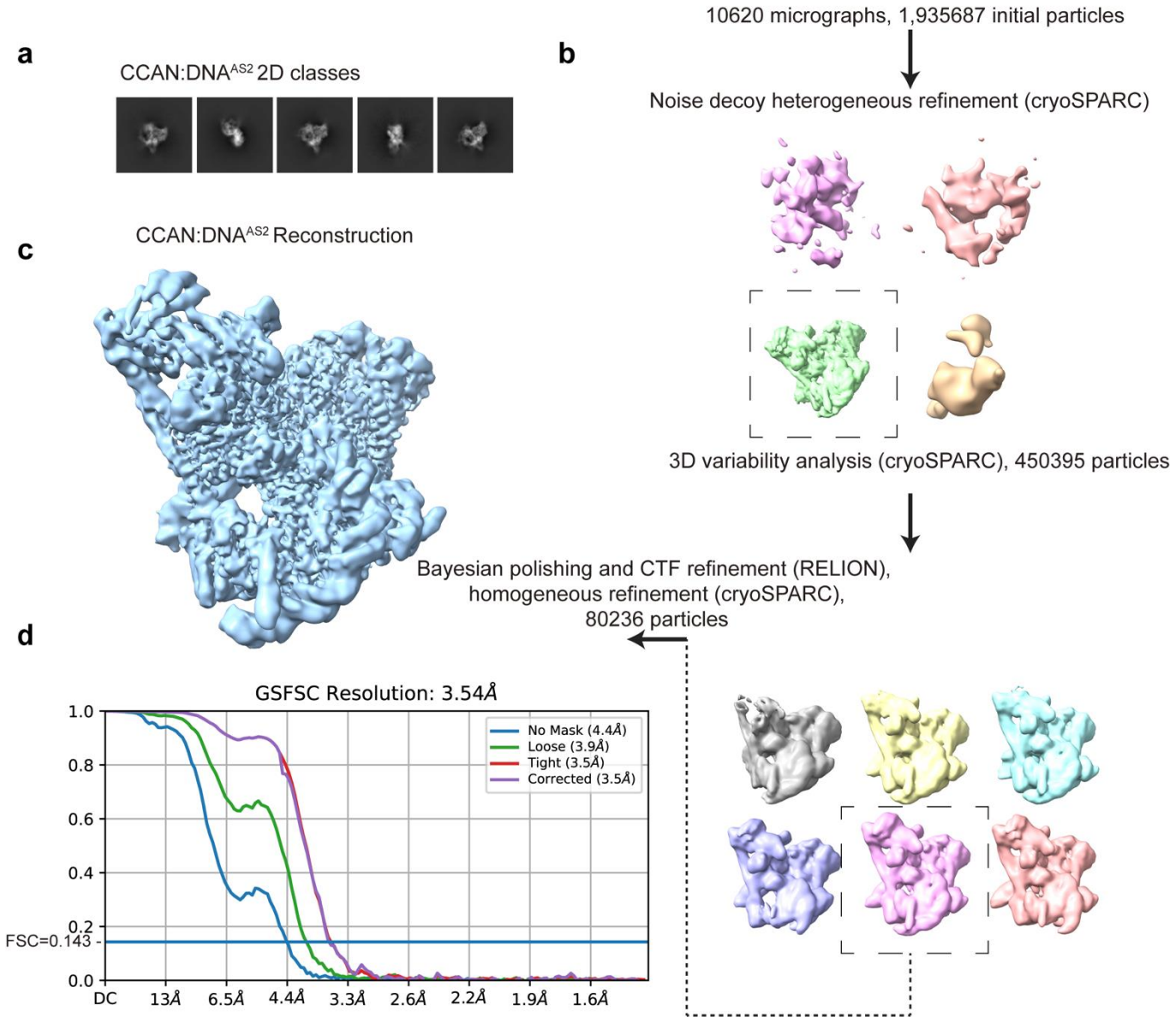

Extended Data Fig. 1. Cryo-EM data and processing workflow for the CCAN:DNA complex. **a**, 2D class averages and FSC curves for CCAN:DNA. **b**, Cryo-EM processing workflow. **c**, 3D reconstruction. **d**, FSC curves.

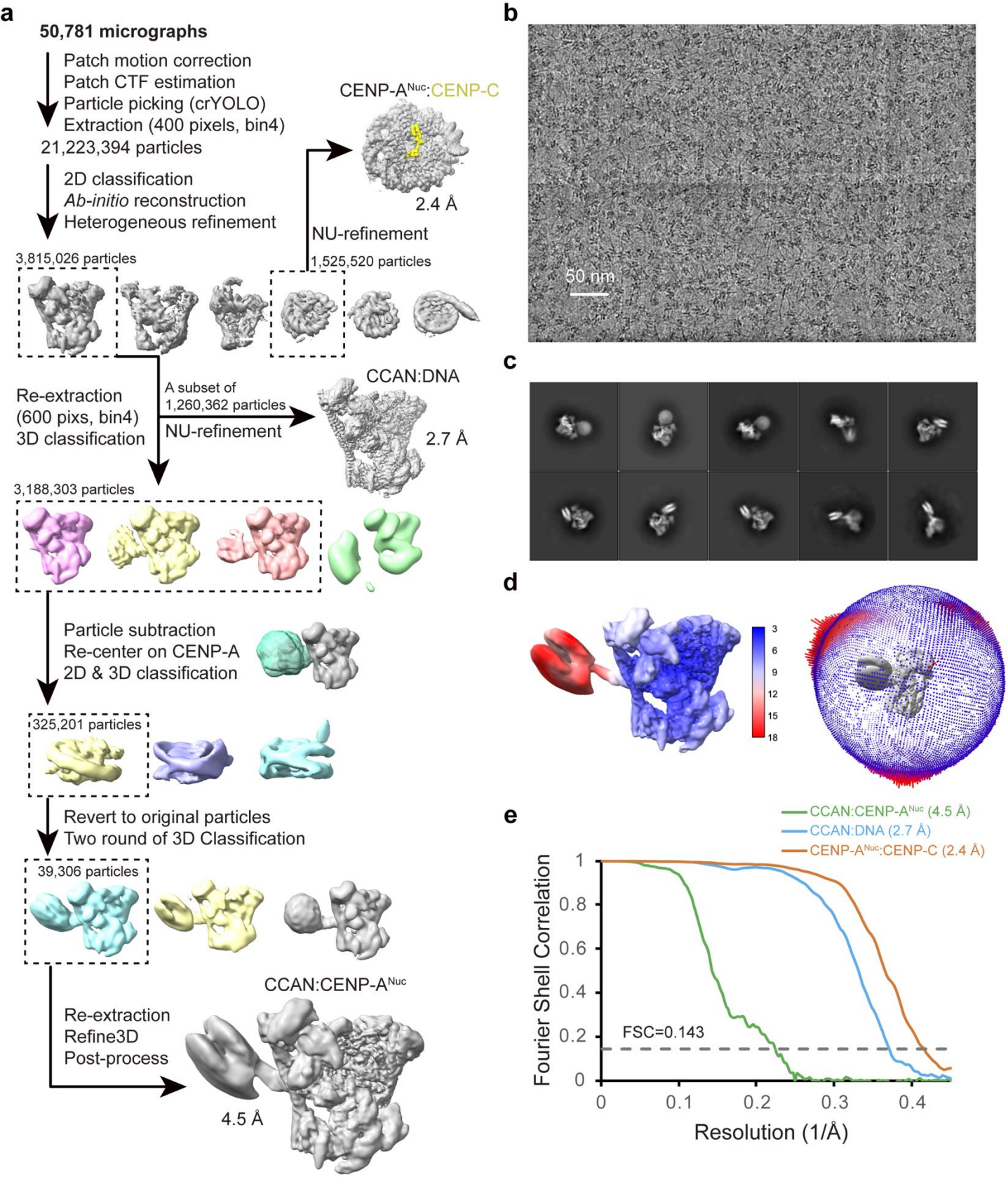

Extended Data Fig. 2. Cryo-EM images and processing workflow for CCAN:CENP-A^{Nuc} complex. **a**, Cryo-EM processing workflow. **b**, Cryo-EM images. **c**, 2D class average gallery. **d**, Cryo-EM reconstruction colour-coded according to local resolution. **e**, FSC curves.

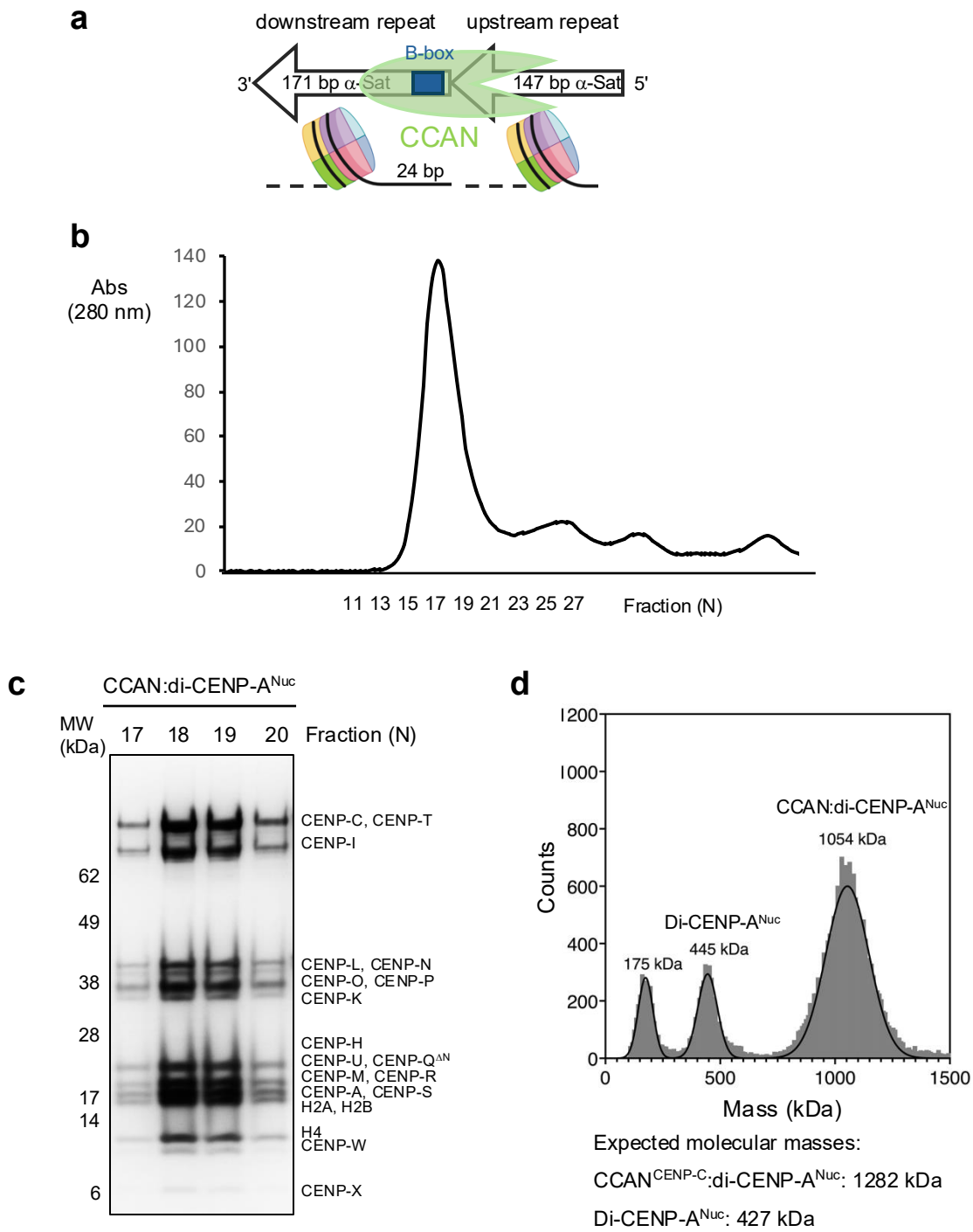

Extended Data Fig. 3. Reconstitution of CCAN:di-CENP-A^{Nuc} complex. a, Schematic of CCAN:di-CENP-A^{Nuc} complex showing α-satellite repeat dimer used in this study. The 3' (downstream) repeat is 171 bp whereas the 5' upstream repeat is 147 bp, i.e. without linker DNA. This design ensures only one CCAN-binding linker DNA per α-satellite repeat dimer. **b** and **c**, Size exclusion chromatogram (b) and associated SDS PAGE gel (c) of purified CCAN:di-CENP-A^{Nuc} complex. **d**, iSCAT data for CCAN:di-CENP-A^{Nuc} complex showing a mixture of di-CENP-A^{Nuc} alone (445 kDa) and the CCAN:di-CENP-A^{Nuc} complex (1,054 kDa).

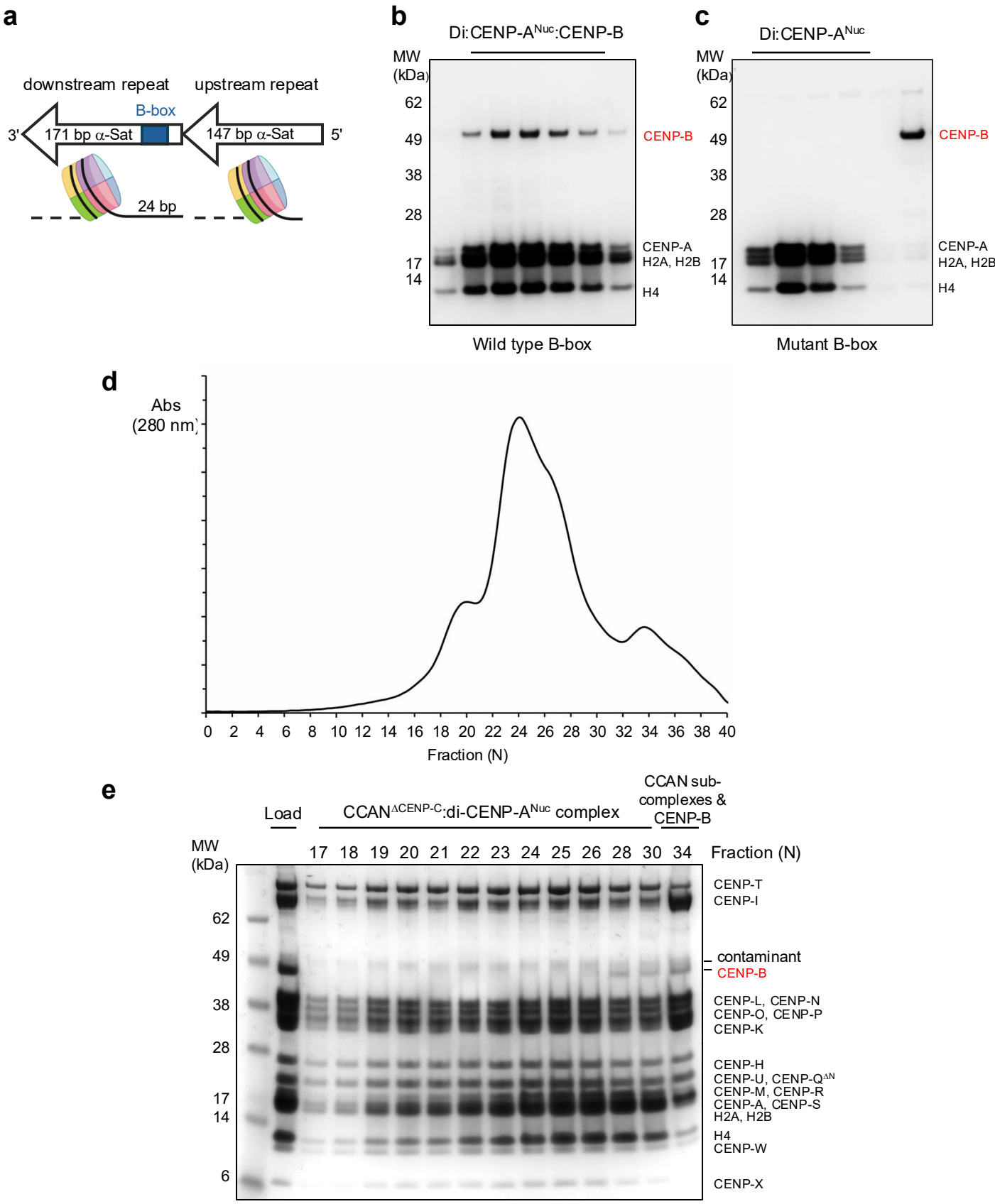

Extended Data Fig. 4. CCAN association with linker DNA displaces CENP-B bound to linker DNA B-box. a, Schematic of the CCAN:di-CENP-A^{Nuc} complex showing a-satellite repeat dimer used in this study with B-box in blue. **b**, Di-CENP-A^{Nuc}:CENP-B complex (with wild type B-box). **c**, CENP-B does not bind to di-CENP-A^{Nuc} with a mutated B-box, demonstrating linker DNA binding. **d**, and **e**, Size exclusion chromatogram (d) and associated SDS PAGE gel (e) showing that CCAN binding to di-CENP-A^{Nuc} displaces CENP-B.

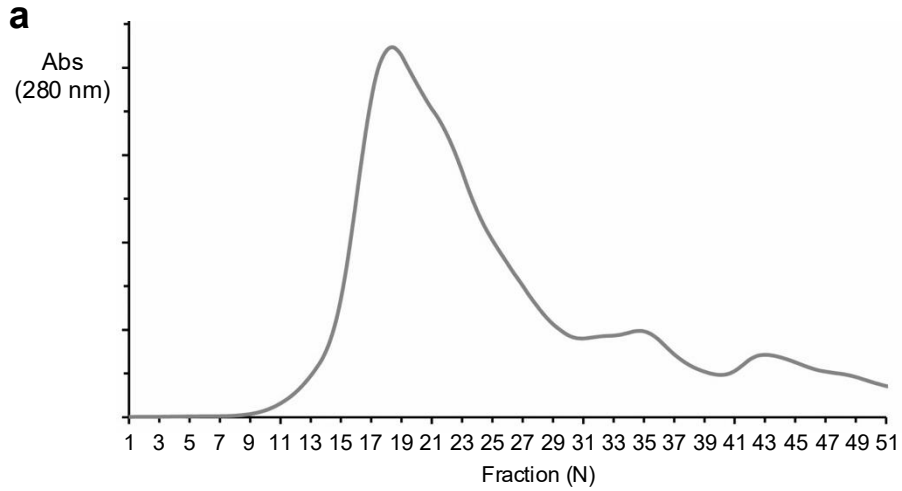

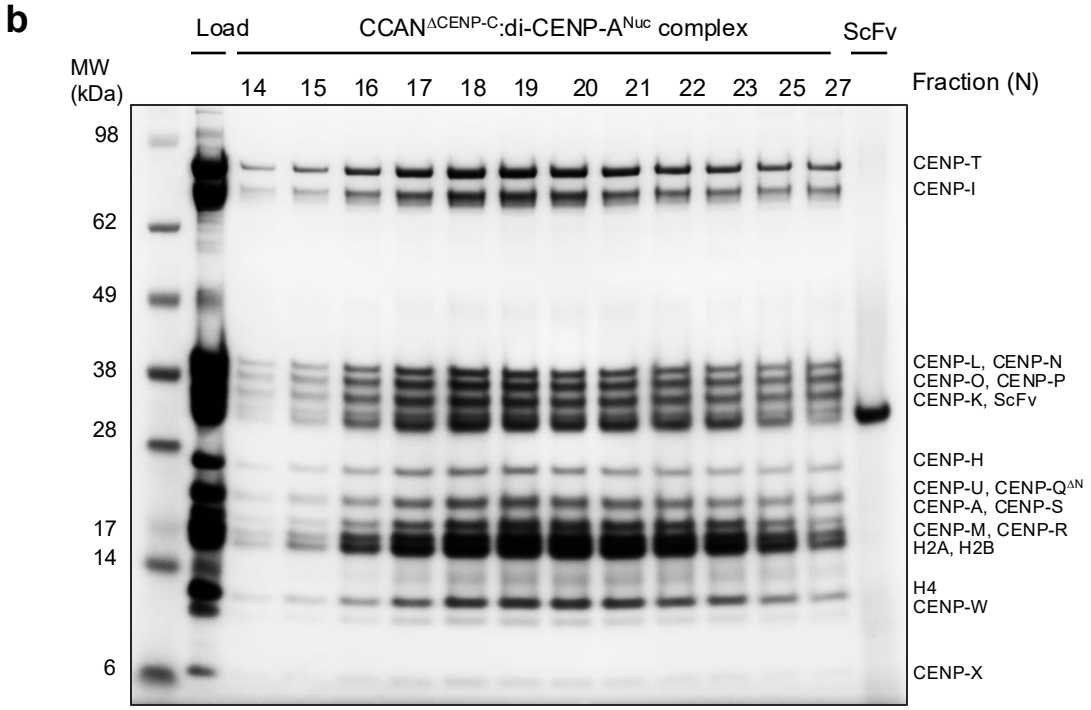

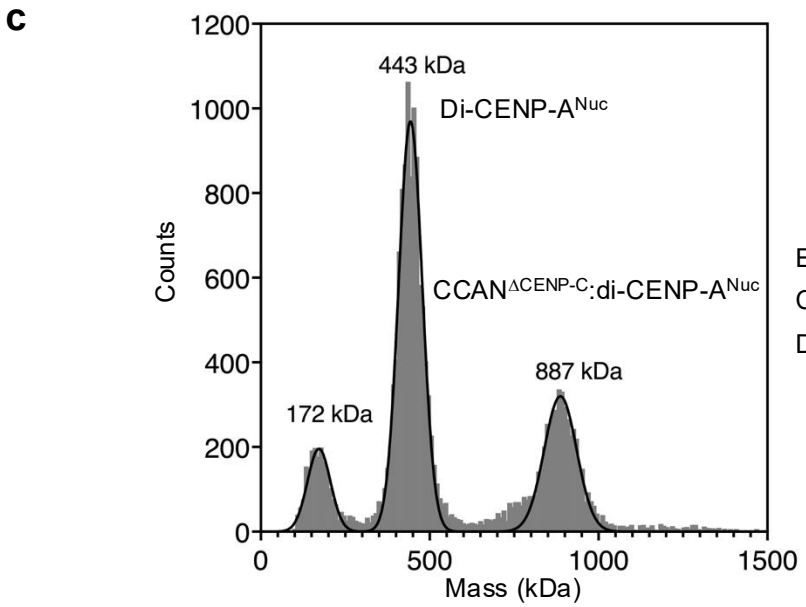

Expected molecular masses:

CCAN$^{\Delta CENP-C}$:di-CENP-A^{Nuc}: 1004 kDa

Di-CENP-A^{Nuc}: 427 kDa

Extended Data Fig. 5. Reconstitution of CCAN$^{DCENP-C}$:di-CENP-A^{Nuc} complex for cryo-EM. a and **b**, Size exclusion chromatogram (A) and associated SDS PAGE gel (B) of purified CCAN$^{\Delta CENP-C}$:di-CENP-A^{Nuc}:ScFv complex. **c**, iSCAT data for CCAN$^{DCENP-C}$:di-CENP-A^{Nuc}:ScFv complex.

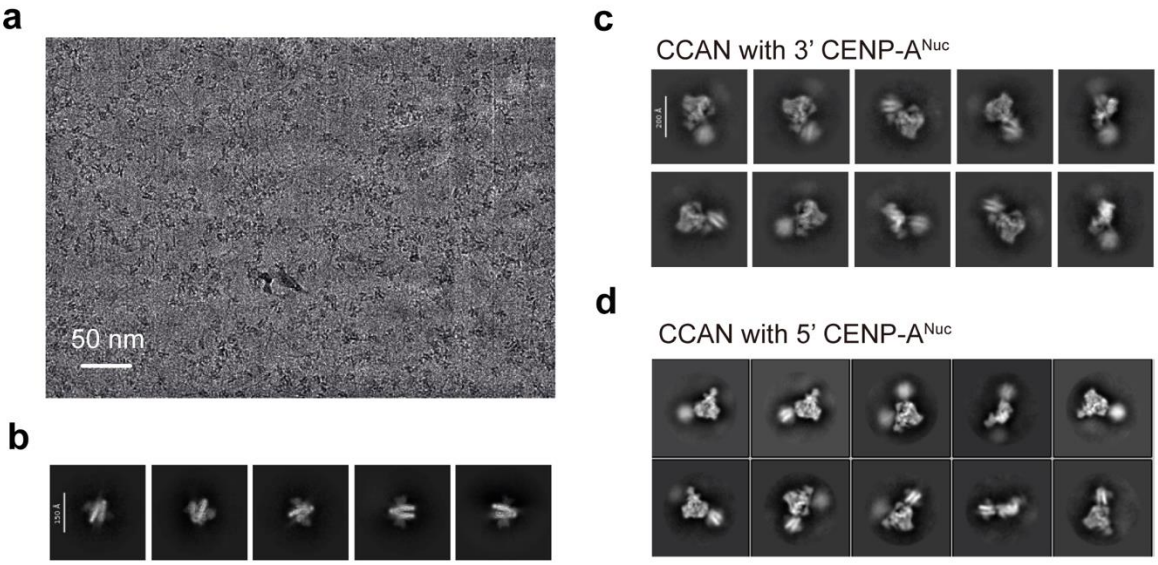

Extended Data Fig. 6. Cryo-EM data for the CCAN:di-CENP-A^{Nuc} complex.
a, Representative cryo-electron micrograph. **b**, 2D class averages of CENP-A^{Nuc}.
c, 2D class averages of CCAN with 3' CENP-A^{Nuc}. **d**, 2D class averages of CCAN with 5' CENP-A^{Nuc}.

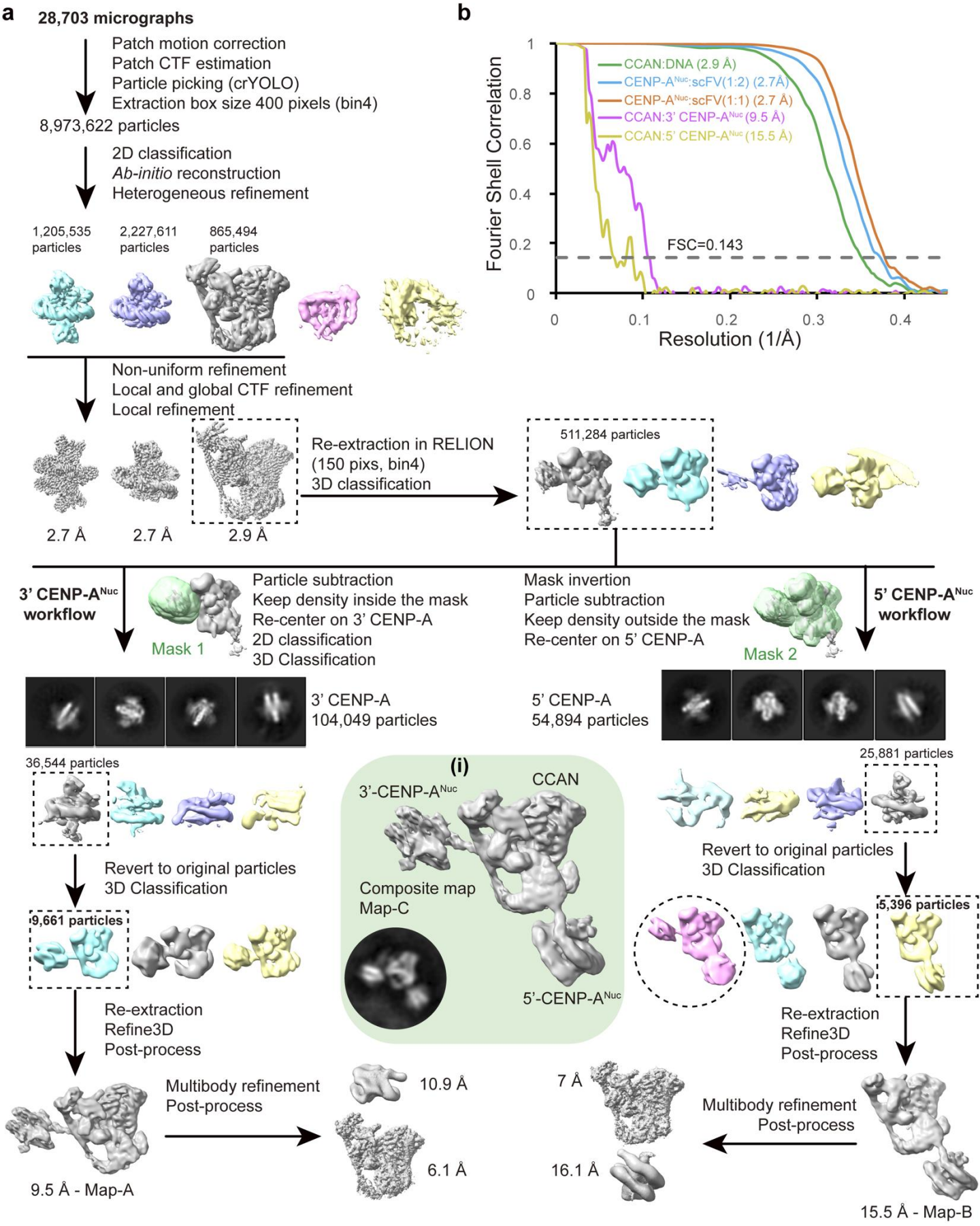

Extended Data Fig. 7. Cryo-EM workflow for CCAN$^{DCENP-C}$:di-CENP-A^{Nuc}:ScFv complex reconstruction. a, Cryo-EM processing workflow. **b**, FSC curves.